

The effect of multiple features on the power spectrum in two-field inflation

K. Boutivas, I. Dalianis, G.P. Kodaxis and N. Tetradis

Department of Physics, University of Athens, University Campus, Zographou 157 84, Greece

E-mail: kboutivas@phys.uoa.gr, idalianis@phys.uoa.gr,
gekontax@phys.uoa.gr, ntetrad@phys.uoa.gr

ABSTRACT: We extend our previous work on the enhancement of the curvature spectrum during inflation to the two-field case. We identify the slow-roll parameter η as the quantity that can trigger the rapid growth of perturbations. Its two components, η_{\parallel} along the background trajectory and η_{\perp} perpendicular to it, remain small during most of the evolution, apart from short intervals during which they take large, positive or negative, values. The typical reason for the appearance of strong features in η_{\parallel} is sharp steps or inflection points in the inflaton potential, while η_{\perp} grows large during sharp turns in field space. We focus on the additive effect of several features leading to the resonant growth of the curvature spectrum. Three or four features in the evolution of η are sufficient in order to induce an enhancement of the power spectrum by six or seven orders of magnitude, which can lead to the significant production of primordial black holes and stochastic gravitational waves. A big part of our study focuses on understanding the evolution of the perturbations and the resulting spectra through analytic means. The presence of multiple features in the background evolution points to a more complex inflationary paradigm, which is also more natural in the multi-field case. The critical examination of this possibility is within the reach of experiment.

Contents

1	Introduction	1
2	Cosmological perturbations in two-field inflation	4
2.1	Background evolution	4
2.2	Perturbations	5
3	Steps or inflection points	7
3.1	Integral equations and an alternative formulation	7
3.2	Analytical expressions for “pulses”	9
3.3	Multiple features	13
4	Turns in field space	13
4.1	Maximal turn and multiple features	14
4.2	The qualitative features of the evolution	15
4.3	Numerical evaluation of the spectra	18
5	GWs and the PBH counterpart	21
6	Summary and conclusions	23
A	Accuracy of the analytical estimates	25
B	An alternative formulation in the two-field case	27

1 Introduction

In the theory of cosmic inflation the cosmological perturbations originate from the quantum fluctuations of the fields that drive inflation [1–4]. The quantum fluctuations of the Bunch-Davies vacuum are stretched at macroscopic scales beyond the Hubble radius and become the seeds for the growth of structure in the universe after inflation ends. The evolution of the fluctuations on the quasi-de Sitter background is affected by the deviations from scale invariance. Strong features in the background can leave characteristic imprints on the spectrum of perturbations with observable consequences. The CMB anisotropies and the large-scale structure of the universe offer us a window to the profile of the spectrum of the primordial perturbations generated in the early stages of inflation [5]. Perturbations generated during the later stages are not imprinted on the CMB sky. However, such small-scale inhomogeneities might be of particular importance if their amplitude is large. A web of strong density perturbations generates a stochastic gravitational wave (GW) background, potentially observable by operating or designed experiments that cover different frequency bands, ranging from nanohertz [6–11] to milihertz and decihertz [12–18], and up to 10^3 hertz [19, 20]. Overdensities with amplitudes beyond a particular threshold collapse into black holes that contribute to the dark matter density. Interestingly enough, if these black holes are in the stellar-mass region, they may be probed by the LIGO-Virgo-KAGRA GW experiments.

The nature of the inflaton field that generates the perturbations remains elusive. Actually, it might be the case that the inflationary phase is implemented by more than one fields. Both single

and multi-field inflation models can describe well the cosmological data of primordial perturbations, assuming that the latter make their multi-field dynamics manifest at scales smaller than those directly observed in the CMB sky. The phenomenology of interest in multi-field inflation models is related to the fact that the curvature perturbations can evolve even on super-Hubble scales because of the presence of isocurvature perturbations [21–27], called also entropy perturbations or non-adiabatic pressure perturbations [28–31]. In particular inflationary set-ups, the evolution of the curvature perturbations triggered by isocurvature modes can be dramatic, generating an observable GW signal and potentially a significant primordial black hole (PBH) abundance [32–35]. At the same time, the isocurvature modes can be absent at the CMB scales $\gtrsim 1$ Mpc, where the curvature perturbations are effectively described by single-field results.

From a particle-physics point of view, it is natural to expect multi-field dynamics during inflation. When more than one fields are rolling, one can define an adiabatic perturbation component along the direction tangent to the background classical trajectory, and isocurvature perturbation components along the directions orthogonal to the trajectory [26]. Curvature perturbations may be affected by the isocurvature perturbations if the background solution follows a curved trajectory in field space. Models of inflation with curved inflaton trajectories have been studied often in the past [33, 34, 36–53]. When the inflaton slow-rolls along a deep valley while the mass term perpendicular to the trajectory is large, the isocurvature perturbation can be integrated out. This introduces corrections to the effective single-field theory, which can be absorbed in the sound speed for the low-energy perturbations [54–58]. In the particular case of a sharp turn in field space [36–44], the impact of the isocurvature modes is more prominent, with the resulting curvature spectrum departing significantly from scale invariance. An oscillatory pattern emerges at wavenumbers characteristic of the turn [39, 40]. Also, a significant amplification takes place if during the sharp turn the isocurvature modes experience a transition from heavy to light [33, 34, 52, 59]. For broader turns the amplification is still possible [50, 51], but the oscillatory patterns fade away.

In this paper we extend our previous work by going beyond the single-field inflationary scenario. We concentrate on the case of two fields that experience strong features in the course of the inflationary evolution. With the term feature we mean sharp deviations from the minimal and smooth inflationary evolution that have observable consequences, such as distinctive signatures in the power spectra of perturbations, see for example refs. [60–62]. The origin of the features is attributed to the intrinsic and complex dynamics of the system of inflaton fields. Aiming at a general and model-independent analysis, we follow an effective description, parameterizing the dynamics behind the strong features via the background evolution encoded in the slow-roll parameters. This phenomenological description also helps to maintain a geometrical intuition about the field space trajectory. Suggestive constructions that capture the dynamics of the subtle underlying mechanisms that produce these features can be inversely engineered. Particular set ups such as those of refs. [53, 63, 64], just to mention a few, indicate some model building directions.

We focus on two particular kinds of strong dynamical features, arising either from sharp steps in the potential or turns in the inflationary trajectory. Such brief but strong departures from a steady slow-roll evolution act as a source for the curvature perturbations, which can be amplified significantly. Even though the two features seem quite distinct, they have a similar description at the level of the slow-roll parameters. This becomes apparent if we decompose, along with the perturbations, the second slow-roll parameter into its tangent η_{\parallel} and orthogonal η_{\perp} components. Sharp steps lead to large positive values of η_{\parallel} , while sharp turns result in large values of η_{\perp} , with either sign. We examine each case separately. Allowing both η_{\parallel} and η_{\perp} to become large leads to a combination of effects, but no new qualitative behaviour. When the leading effect comes from the rapid change of the η_{\parallel} component, the inflationary dynamics is effectively described by a single-field theory. A step-like transition in the inflaton potential energy can cause this change. We studied this possibility in previous work, following mainly a numerical approach [65, 66]. We extend this

work here by focusing on the analytic understanding of the evolution of the perturbations and the resulting spectra. In the second case we study, the η_{\perp} component is rapidly changing when a turn in field space takes place. In this case it is the isocurvature perturbations that get excited. Through their coupling to the curvature perturbations, which is proportional to η_{\perp} , they play a crucial role in shaping the final curvature spectrum.

In the case of large η_{\parallel} , we calculate the power spectrum of curvature perturbations following a semi-analytic approach. The conventional perturbative approach has limitations because the equations of motion can be solved analytically only when the slow-roll parameters have a mild time dependence within the slow-roll approximation. We utilize here the Green's function method in order to recast the system of equations of motion for the fields in a form that admits an iterative solution. We also find a formula that gives an approximate solution in closed form. For a moderate enhancement of the slow-roll parameter our formalism can give a good quantitative description of the evolution of the curvature perturbation. This formalism can also describe other features, such as an inflection point in the inflaton potential. It can be extended to the two-field case, even though the resulting expressions are rather complicated. The semi-analytic approach has several advantages over a purely numerical treatment: one can read off characteristic frequencies, analyze non-minimal initial conditions in a straightforward manner, and reduce computational time. However, the quantitative accuracy is limited to enhancements of the curvature power spectrum up to three or four orders of magnitude. For larger enhancements our approximation captures well the characteristic frequencies, but not the exact size of the amplification. In this case the numerical solution for the system of equations of motion is necessary.

For the two-field inflation system with a transient large value of η_{\perp} , a strong enhancement of the curvature spectrum is possible. Previous studies have concluded that an enhancement by several orders of magnitude can be achieved only for a nonzero curvature of the internal manifold spanned by the fields [33, 34]. This would require noncanonical kinetic terms. We show that a large enhancement can take place even for vanishing internal curvature if there are several instances during which η_{\perp} grows large. Such a situation would occur if, for example, the two-field system experiences several sharp turns during its evolution. The mechanism for the enhancement is different from the case of a single large- η_{\perp} event and leads to spectra with a different profile. For this reason our analysis and results differ from previous studies in this subject, in which the assumption of a non-trivial field-space metric was the essential ingredient. More specifically, we find that a system of two fields with canonical kinetic terms can source large curvature perturbations if there are a few turns in the background trajectory, each taking place in a time interval less than a Hubble time. We consider turns smaller than π with alternating signs, so that the field trajectory does not cross itself. Three or four turns are sufficient to enhance the curvature power spectrum by a factor of 10^7 . A larger number of rather small but sharp turns can produce an equally large enhancement. We assume that these features occur at intermediate or late stages of the inflationary evolution, so that the spectrum in the CMB range remains unaffected.

The fact that a prominent peak in the density spectrum is generated implies that a strong GW signal is also induced at the moment of horizon reentry. The GW channel is a portal to the primordial density perturbations at small scales and can probe the inflationary dynamics. Hence, along with the excited curvature power spectra we present the corresponding tensor power spectra induced at second order in perturbation theory [67–70]. We find that at least three turns are required in order for the induced GW signal to be strong enough to be detected. Large fluctuations of the curvature perturbation can trigger gravitational collapse, which, though an extremely rare event, becomes important above a particular threshold [71]. For completeness we consider the corresponding PBH production for two benchmark mass values and PBH abundances that can be tested by current and near future GW experiments.

The paper is organized as follows: In section 2 we present the background evolution of the

two-field inflaton system, as well as the evolution of the cosmological perturbations, including the interaction between isocurvature and curvature modes. In section 3 we present approximate analytic solutions for the first class of strong features that result from steps and inflection points in the potential. In section 4 we analyze the second class of features that result from sharp turns in field space. In section 5 we present the tensor spectra and the PBH counterpart, focusing on the case in which the final curvature perturbation originates almost exclusively in the interactions with the isocurvature modes. In section 6 we present our conclusions. In appendix A we provide an assessment of the accuracy of analytical estimates of the spectrum presented in the main text. In appendix B we give some detailed expressions resulting from the application of the Green's function method to the two-field system.

2 Cosmological perturbations in two-field inflation

2.1 Background evolution

The action is of the form

$$S = \int d^4x \sqrt{-g} \left[\frac{1}{2}R - \frac{1}{2}g^{\mu\nu} \gamma_{ab} \partial_\mu \phi^a \partial_\nu \phi^b - V(\phi) \right], \quad (2.1)$$

with $a = 1, 2$. We have chosen units such that the Planck mass is $M_{\text{Pl}} = 1$. On an expanding, spatially flat background, with scale factor $a(t)$, the equations of motion of the background fields take the form [40, 58]

$$\frac{D}{dt} \dot{\phi}^a + 3H \dot{\phi}^a + V^a = 0 \quad (2.2)$$

$$3H^2 = \frac{1}{2} \dot{\phi}^2 + V, \quad (2.3)$$

where $V^a = \gamma^{ab} \partial V / \partial \phi^b$, $H = \dot{a}/a$, with a dot denoting a derivative with respect to cosmological time, and

$$\frac{D}{dt} X^a = \dot{X}^a + \Gamma_{bc}^a \dot{\phi}^b X^c. \quad (2.4)$$

By defining $\dot{\phi}^2 \equiv \gamma_{ab} \dot{\phi}^a \dot{\phi}^b$, we obtain

$$\dot{H} = -\frac{\dot{\phi}^2}{2}. \quad (2.5)$$

We next define vectors T^a and N^a tangent and normal to the path

$$T^a = \frac{\dot{\phi}^a}{\dot{\phi}} \quad (2.6)$$

$$N_a = (\det \gamma)^{1/2} \epsilon_{ab} T^b, \quad (2.7)$$

such that $T^a T_a = N^a N_a = 1$, $T^a N_a = 0$. Projecting eq. (2.2) along T^a , one finds

$$\ddot{\phi} + 3H \dot{\phi} + V_T = 0, \quad (2.8)$$

where $V_T = T^a \partial V / \partial \phi^a$. One also finds

$$\frac{DT^a}{dt} = -\frac{V_N}{\dot{\phi}} N^a, \quad (2.9)$$

with $V_N = N^a \partial V / \partial \phi^a$. The slow-roll parameters are defined as

$$\epsilon \equiv -\frac{\dot{H}}{H^2} = \frac{\dot{\phi}^2}{2H^2} \quad (2.10)$$

$$\eta^a \equiv -\frac{1}{H \dot{\phi}} \frac{D \dot{\phi}^a}{dt}. \quad (2.11)$$

Then η^a can be decomposed as

$$\eta^a = \eta_{\parallel} T^a + \eta_{\perp} N^a, \quad (2.12)$$

with

$$\eta_{\parallel} = -\frac{\ddot{\phi}}{H\dot{\phi}} = -\frac{\dot{\epsilon}}{2H\epsilon} + \epsilon \quad (2.13)$$

$$\eta_{\perp} = \frac{V_N}{H\dot{\phi}}. \quad (2.14)$$

We also have

$$\frac{DT^a}{dt} = -H\eta_{\perp} N^a \quad (2.15)$$

$$\frac{DN^a}{dt} = +H\eta_{\perp} T^a. \quad (2.16)$$

2.2 Perturbations

The evolution equations for the curvature and isocurvature perturbations in two-field inflation can be cast in the form [40, 58]

$$\mathcal{R}_{k,NN} + (3 + \epsilon - 2\eta_{\parallel}) \mathcal{R}_{k,N} + \frac{k^2}{H^2} e^{-2N} \mathcal{R}_k = -2 \frac{\eta_{\perp}}{\sqrt{2\epsilon}} [\mathcal{F}_{k,N} + (3 - \eta_{\parallel} - \xi_{\perp}) \mathcal{F}_k] \quad (2.17)$$

$$\mathcal{F}_{k,NN} + (3 - \epsilon) \mathcal{F}_{k,N} + \frac{k^2}{H^2} e^{-2N} \mathcal{F}_k + \left(\frac{M^2}{H^2} + \epsilon \mathbb{R} - \eta_{\perp}^2 \right) \mathcal{F}_k = 2\sqrt{2\epsilon} \eta_{\perp} \mathcal{R}_{k,N}, \quad (2.18)$$

with

$$\eta_{\parallel} = \epsilon - \frac{\epsilon, N}{2\epsilon} \quad (2.19)$$

$$\xi_{\perp} = -\frac{\eta_{\perp, N}}{\eta_{\perp}}. \quad (2.20)$$

We have written the equations in Fourier space, using the number of efoldings N as independent variable. The subscripts denote derivatives with respect to N . Here \mathcal{R}_k is the curvature perturbation, while \mathcal{F}_k is related to the isocurvature perturbation \mathcal{S} through $\mathcal{F}_k = \sqrt{2\epsilon} \mathcal{S}_k$. The mass M of the isocurvature perturbation is given by the curvature of the potential in the direction perpendicular to the trajectory of the background inflaton. The variable \mathbb{R} is the Ricci scalar of the internal manifold spanned by the scalar fields [22]. It vanishes for a model with standard kinetic terms for the two fields.

In order to focus on the main features associated with the enhancement of the curvature spectrum, we make some simplifying assumptions:

- We approximate the Hubble parameter as constant. This is a good approximation, as its variation during the period of interest is $\mathcal{O}(10\%)$, while the spectrum may increase by several orders of magnitude.
- In a similar vein, we take the mass M of the isocurvature modes to be constant. We also assume that $M \gtrsim H$, so that the isocurvature perturbations are suppressed apart from short periods during which the parameter η_{\perp} becomes large.
- We do not consider the possibility of a curved field manifold, but assume that the fields have standard kinetic terms. This means that we can set $\mathbb{R} = 0$.

- We assume that the parameter ϵ takes a small constant value while the system is in the slow-roll regime, consistently with the constraints from the cosmic microwave background (CMB). We neglect here corrections arising from the slow-roll regime that lead to small deviations from scale invariance. We focus instead on short periods of the inflaton evolution during which η_{\parallel} or η_{\perp} can grow large. These periods are reflected in strong deviations of the spectrum from scale invariance over a range of momentum scales.

We are interested in strong deviations from the slow-roll regime during short intervals in N , which can result in the strong enhancement of the curvature perturbations. There are two typical scenarios that we have in mind:

- For $\eta_{\perp}^2 \ll M^2/H^2$, the isocurvature mode is strongly suppressed and the rhs of eq. (2.17) vanishes. The curvature mode can be enhanced if the coefficient of the term $\sim \mathcal{R}_{k,N}$ in the lhs becomes negative. This requires large positive values of the parameter η_{\parallel} . Such values can be attained if the inflaton potential displays an inflection point, or a sharp step [65, 66]. The dominant effect comes from η_{\parallel} , which can take very large values, while ϵ takes values at most around 1 and can be neglected. The equation for the curvature perturbation can be approximated as

$$\mathcal{R}_{k,NN} + (3 - 2\eta_{\parallel}) \mathcal{R}_{k,N} + \frac{k^2}{H^2} e^{-2N} \mathcal{R}_k = 0. \quad (2.21)$$

- If $\eta_{\perp}^2 \gg M^2/H^2$ for a short period, the isocurvature modes can be temporarily excited very strongly. The rhs of eq. (2.17) then becomes large and acts as a source for the curvature perturbations, leading to their strong enhancement. At a later time, η_{\perp} becomes small and the isocurvature perturbations become suppressed again. This process can take place while the slow-roll parameters ϵ and η_{\parallel} remain small. In order to capture the essence of this mechanism, we assume that ϵ is small and roughly constant, and switch to the field $\mathcal{S}_k = \mathcal{F}_k/\sqrt{2\epsilon}$. The system of eqs. (2.17), (2.18) becomes

$$\mathcal{R}_{k,NN} + 3\mathcal{R}_{k,N} + \frac{k^2}{H^2} e^{-2N} \mathcal{R}_k = -2(\eta_{\perp} \mathcal{S}_{k,N} + \eta_{\perp,N} \mathcal{S}_k + 3\eta_{\perp} \mathcal{S}_k) \quad (2.22)$$

$$\mathcal{S}_{k,NN} + 3\mathcal{S}_{k,N} + \frac{k^2}{H^2} e^{-2N} \mathcal{S}_k + \left(\frac{M^2}{H^2} - \eta_{\perp}^2 \right) \mathcal{S}_k = 2\eta_{\perp} \mathcal{R}_{k,N}. \quad (2.23)$$

Notice that \mathcal{S}_k is the appropriate field on which the initial condition of a Bunch-Davies vacuum can be imposed, similarly to \mathcal{R}_k .

In both the above scenarios, it is the acceleration in the evolution of the background inflaton, either in the direction of the flow through $\eta_{\parallel}(N)$, or perpendicularly to it through $\eta_{\perp}(N)$, that causes the amplification of the spectrum of curvature perturbations. Another common characteristic is that the spectrum displays strong oscillatory patterns.

A weak point of the above scenarios is that the enhancement of the curvature spectrum by several orders of magnitude can be achieved only under special conditions. The inflaton potential around an inflection point must be fine-tuned with high accuracy [72–75]. A step in the potential gives a limited enhancement, unless the potential is engineered in a very specific way [76]. Finally, a sharp turn in the inflaton trajectory must reach a value of 4π for the enhanced spectrum to have observable consequences [33]. This is possible only if the field manifold is curved.

Our aim is to demonstrate that a strong enhancement of the curvature spectrum is possible if several strong features in the inflaton potential combine constructively. For example, a sequence of steps or turns in field space, that occur within a small number of efoldings, can lead to an effect on the spectrum that exceeds the effect of one feature by several orders of magnitude.

3 Steps or inflection points

In this section we analyze the scenario in which $\eta_{\perp}^2 \ll M^2/H^2$ during the whole evolution. The isocurvature mode is always suppressed and the single relevant perturbation can be identified with the curvature mode. Its evolution is governed by eq. (2.21). This equation has been discussed in refs. [65, 66] in the context of single-field inflation, where oscillatory patterns have been observed. In single-field setups oscillatory behaviour in specific parts of the spectrum has been also observed in ref. [77]. Our aim here is to obtain a better analytic understanding of the nature of the solutions and the resulting form of the spectrum. We focus mainly on inflaton potentials that display one or more steps, which have been shown to result in power spectra of curvature perturbations that can be strongly enhanced within a certain momentum range relative to the scale invariant case.

3.1 Integral equations and an alternative formulation

For a general form of the function $\eta_{\parallel}(N)$, we rewrite eq. (2.21) as

$$R_{k,NN} + 3R_{k,N} + \frac{k^2}{e^{2N}H^2}R_k = 2\eta_{\parallel}(N)R_{k,N}. \quad (3.1)$$

The Green's function $G(N, n)$ for the operator in the lhs satisfies the equation

$$G_{k,NN}(N, n) + 3G_{k,N}(N, n) + \frac{k^2}{e^{2N}H^2}G_k(N, n) = \delta(N - n). \quad (3.2)$$

The evolution is classical, so we must use the retarded Green's function, which satisfies $G_{k>}(N, n) = 0$ for $n > N$. For $n < N$ the solution is

$$G_{k<}(N, n) = e^{-\frac{3}{2}N} \left(A(n)J_{3/2} \left(e^{-N} \frac{k}{H} \right) + B(n)J_{-3/2} \left(e^{-N} \frac{k}{H} \right) \right). \quad (3.3)$$

The Green's function is continuous at $N = n$. Its first derivative has a discontinuity, obtained by integrating eq. (3.2) around $N = n$. This gives $G_{k<,N}(n, n) = 1$. Imposing these constraints gives

$$A(n) = -\sqrt{\frac{\pi}{2}}e^{3n} \left(\frac{k}{H} \right)^{-3/2} \left(\cos \left(e^{-n} \frac{k}{H} \right) + e^{-n} \frac{k}{H} \sin \left(e^{-n} \frac{k}{H} \right) \right) \quad (3.4)$$

$$B(n) = \sqrt{\frac{\pi}{2}}e^{3n} \left(\frac{k}{H} \right)^{-3/2} \left(e^{-n} \frac{k}{H} \cos \left(e^{-n} \frac{k}{H} \right) - \sin \left(e^{-n} \frac{k}{H} \right) \right). \quad (3.5)$$

Then, the solution of eq. (3.1) is

$$R_k(N) = \bar{R}_k(N; 1, i, 3) + 2 \int_{-\infty}^N G_k(N, n) \eta_{\parallel}(n) R_{k,n}(n) dn, \quad (3.6)$$

with $\bar{R}_k(N; C_p, C_m, \kappa)$ given by

$$\bar{R}_k(N; C_p, C_m, \kappa) = A_0 e^{-\frac{1}{2}\kappa N} \left(C_p J_{\kappa/2} \left(e^{-N} \frac{k}{H} \right) + C_m J_{-\kappa/2} \left(e^{-N} \frac{k}{H} \right) \right). \quad (3.7)$$

The values $\kappa = 3$, $C_p = 1$, $C_m = i$ correspond to the Bunch-Davies vacuum.

An approximate expression, which can be considered as the first step in an iterative solution of the above equation, can be obtained if we replace the full solution $R_k(n)$ in the integral with $\bar{R}_k(n, 1, i, 3)$. This gives [66]

$$R_k(\infty) = \bar{R}_k(\infty; 1, i, 3) \times \left\{ 1 - 2i \frac{H}{k} \int_{-\infty}^{\infty} \eta_{\parallel}(n) e^n \left[e^{-n} \frac{k}{H} \cos \left(e^{-n} \frac{k}{H} \right) - \sin \left(e^{-n} \frac{k}{H} \right) \right] \left[i \cos \left(e^{-n} \frac{k}{H} \right) - \sin \left(e^{-n} \frac{k}{H} \right) \right] dn \right\}. \quad (3.8)$$

Through a partial integration, we can recast eq. (3.6) as

$$R_k(N) = \bar{R}_k(N; 1, i, 3) - 2 \int_{-\infty}^N \frac{\partial}{\partial n} [G_k(N, n) \eta_{\parallel}(n)] R_k(n) dn, \quad (3.9)$$

where we have used that $G_k(N, N) = 0$ and $\eta_{\parallel}(n) \rightarrow 0$ for $n \rightarrow -\infty$. The form (3.3) of the Green's function suggests the ansatz

$$R_k(N) = e^{-\frac{3}{2}N} \left(D(N) J_{3/2} \left(e^{-N} \frac{k}{H} \right) + E(N) J_{-3/2} \left(e^{-N} \frac{k}{H} \right) \right). \quad (3.10)$$

Substituting in eq. (3.9) and matching the coefficients of the Bessel functions, we obtain

$$D(N) = 1 - \int_{-\infty}^N \frac{\partial}{\partial n} [A(n) 2\eta_{\parallel}(n)] e^{-\frac{3}{2}n} \left[J_{3/2} \left(e^{-n} \frac{k}{H} \right) D(n) + J_{-3/2} \left(e^{-n} \frac{k}{H} \right) E(n) \right] dn \quad (3.11)$$

$$E(N) = i - \int_{-\infty}^N \frac{\partial}{\partial n} [B(n) 2\eta_{\parallel}(n)] e^{-\frac{3}{2}n} \left[J_{3/2} \left(e^{-n} \frac{k}{H} \right) D(n) + J_{-3/2} \left(e^{-n} \frac{k}{H} \right) E(n) \right] dn \quad (3.12)$$

In the first step of an iterative solution of the above equation, one substitutes $D(n) = 1$ and $E(n) = i$ within the integrals in the rhs. For $N \rightarrow \infty$ the solution (3.10) is dominated by the term proportional to $J_{-3/2}$. Making use of a partial integration within the integral in eq. (3.12), we recover the approximate solution (3.8).

In order to improve on this result, we can differentiate the relations (3.11), (3.12) with respect to N , in order to obtain a system of two first-order differential equations:

$$\frac{\partial}{\partial N} \begin{pmatrix} D(N) \\ E(N) \end{pmatrix} = F(N) \begin{pmatrix} D(N) \\ E(N) \end{pmatrix}, \quad (3.13)$$

where

$$F(N) = - \begin{pmatrix} \frac{\partial}{\partial N} [A(N) 2\eta_{\parallel}(N)] e^{-\frac{3}{2}N} J_{3/2} \left(e^{-N} \frac{k}{H} \right) & \frac{\partial}{\partial N} [A(N) 2\eta_{\parallel}(N)] e^{-\frac{3}{2}N} J_{-3/2} \left(e^{-N} \frac{k}{H} \right) \\ \frac{\partial}{\partial N} [B(N) 2\eta_{\parallel}(N)] e^{-\frac{3}{2}N} J_{3/2} \left(e^{-N} \frac{k}{H} \right) & \frac{\partial}{\partial N} [B(N) 2\eta_{\parallel}(N)] e^{-\frac{3}{2}N} J_{-3/2} \left(e^{-N} \frac{k}{H} \right) \end{pmatrix}. \quad (3.14)$$

The matrix $F(N)$ has vanishing determinant. Its nonzero eigenvalue is $2\eta_{\parallel}(N)$. The system of equations (3.13) can be solved numerically with the initial condition $(D(N), E(N)) = (1, i)$ that corresponds to the Bunch-Davies vacuum. This formulation provides an advantage over the numerical solution of eq. (2.21), for which the initial condition is strongly oscillatory. Moreover, it makes it straightforward to analyze alternative assumptions for the vacuum.

The solution of eq. (3.13) can be expressed as

$$\begin{pmatrix} D(N) \\ E(N) \end{pmatrix} = Q(N) \begin{pmatrix} 1 \\ i \end{pmatrix}, \quad (3.15)$$

where $Q(N)$ is the fundamental matrix. An exact analytic determination of $Q(N)$ in closed form is not possible because of the N -dependence of $F(N)$. For a slowly varying $F(N)$ (adiabatic limit), an approximate solution is given by

$$Q(N) = \exp(C(N)), \quad C(N) = \int_{-\infty}^N F(n) dn. \quad (3.16)$$

In appendix A we provide an assessment of the accuracy of the approximate expressions (3.8) and (3.16). Both approximations give a very accurate description of the spectrum when its value is of order 1. When the spectrum is significantly enhanced both approximations lose accuracy. However, eq. (3.16) gives a reasonable approximation to the maximal value of the spectrum and its characteristic frequencies, even for an enhancement by three orders of magnitude.

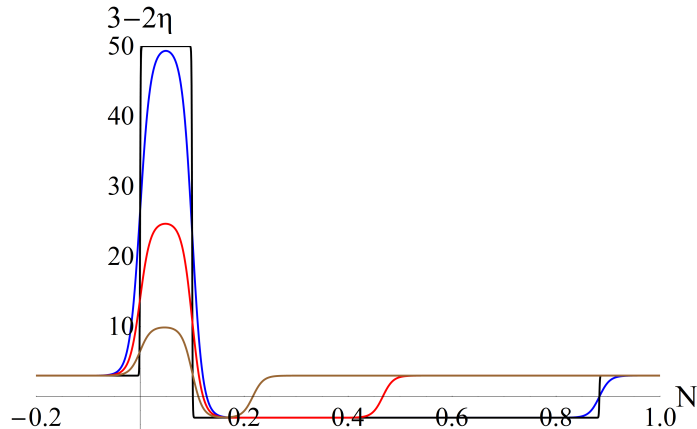


Figure 1. Typical evolution of the function $\eta_{\parallel}(N)$ induced by steps in the inflaton potential.

3.2 Analytical expressions for “pulses”

In order to obtain a better understanding of the characteristic features of the spectrum, we consider a sequence of typical patterns for the function $\eta_{\parallel}(N)$, similar to those induced by step steps in the inflaton potential. The slow-roll parameter first decreases sharply to very negative values during the very short interval that the step is crossed by the background field. Subsequently, the inflaton settles in a slow-roll regime on a flat part of the potential. During the approach to slow-roll, the evolution is dominated by the first two terms in the equation of motion of the background field: $\ddot{\phi} + 3H\dot{\phi} = 0$. This means that we have $\eta_{\parallel} \simeq 3$ during this interval. Eventually, the system returns to slow roll and η_{\parallel} becomes almost zero. It has been shown in refs. [65, 66] that the power spectrum is scale invariant at late times (or $N \rightarrow \infty$) for $k \rightarrow \infty$, but has a value multiplied by the factor [66]

$$\left[\delta\Delta_R^{(\infty)}\right]^2 = \exp\left(2\int_{-\infty}^{\infty}\eta_{\parallel}(N)dN\right), \quad (3.17)$$

relative to its scale-invariant value for modes that have sufficiently small k and freeze before being affected by the features in the potential. For $\eta_{\parallel} < 0$ the spectrum is suppressed, while for $\eta_{\parallel} > 0$ it is enhanced. If the integral is zero, the spectrum for $k \rightarrow \infty$ has the same amplitude as for $k \rightarrow 0$. A different way to understand this effect is to notice that

$$-2\int_{N_e}^{N_l}\eta_{\parallel}(N)dN \simeq 2\log\frac{\epsilon_l}{\epsilon_e}, \quad (3.18)$$

where ϵ_e and ϵ_l are the values of the ϵ parameter on the plateaus of the inflaton potential before and after a strong feature that induces strong deviations from scale invariance. The integral vanishes for a feature localized between regions supporting slow-roll inflation with similar values of ϵ . We impose this constraint on $\eta_{\parallel}(N)$ throughout this work in order to focus solely on the effect of the feature.

In fig. 1 we depict a sequence of smooth functions $\eta_{\parallel}(N)$ with the above characteristics. The evolution is very similar to that typically induced by inflaton potentials with step steps [65, 66]. The maximal value of $3 - 2\eta_{\parallel}$ increases with the steepness of the step, along with the duration of the interval during which $3 - 2\eta_{\parallel} \simeq -3$.

In this subsection we present an analytic approach based on an approximation of the evolution of η_{\parallel} through “pulses”. The essence of this approximation is depicted in fig. 1 by the curve with the very sharp transitions when η_{\parallel} changes value. We name the evolution from vanishing η_{\parallel} to a

nonzero constant value, and back to zero after a period of efoldings, a square “pulse”. For constant $\kappa \equiv 3 - 2\eta_{\parallel}$, the solution of eq. (2.21) involves a linear combination of the Bessel functions $J_{\pm\kappa/2}$ and has the form of eq. (3.7). For $\kappa = 3$ we obtain a scale-invariant spectrum. The Bunch-Davies vacuum corresponds to $C_p = 1$, $C_m = i$. As we have mentioned before, we are interested only in relatively strong deviations from scale invariance, and not in the absolute normalization of the spectrum. For this reason we set $A_0 = 1$.

If κ changes at $N = N_{fi}$ from an initial value κ_i to a new value κ_f , one can compute the change from initial coefficients C_{p_i}, C_{m_i} to new coefficients C_{p_f}, C_{m_f} by requiring the continuity of the solution of eq. (2.21) and its first derivative [66]. The new coefficients are given by

$$\begin{pmatrix} C_{p_f} \\ C_{m_f} \end{pmatrix} = M(N_{fi}, \kappa_i, \kappa_f, k) \begin{pmatrix} C_{p_i} \\ C_{m_i} \end{pmatrix}, \quad (3.19)$$

where the matrix $M(N_{fi}, \kappa_i, \kappa_f, k)$ has components

$$\begin{aligned} M_{11} &= C \left(J_{-\kappa_f/2} \left(e^{-N_{fi}} \frac{k}{H} \right) J_{-1+\kappa_i/2} \left(e^{-N_{fi}} \frac{k}{H} \right) + J_{1-\kappa_f/2} \left(e^{-N_{fi}} \frac{k}{H} \right) J_{\kappa_i/2} \left(e^{-N_{fi}} \frac{k}{H} \right) \right) \\ M_{12} &= C \left(-J_{-\kappa_f/2} \left(e^{-N_{fi}} \frac{k}{H} \right) J_{1-\kappa_i/2} \left(e^{-N_{fi}} \frac{k}{H} \right) + J_{1-\kappa_f/2} \left(e^{-N_{fi}} \frac{k}{H} \right) J_{-\kappa_i/2} \left(e^{-N_{fi}} \frac{k}{H} \right) \right) \\ M_{21} &= C \left(-J_{\kappa_f/2} \left(e^{-N_{fi}} \frac{k}{H} \right) J_{-1+\kappa_i/2} \left(e^{-N_{fi}} \frac{k}{H} \right) + J_{-1+\kappa_f/2} \left(e^{-N_{fi}} \frac{k}{H} \right) J_{\kappa_i/2} \left(e^{-N_{fi}} \frac{k}{H} \right) \right) \\ M_{22} &= C \left(J_{\kappa_f/2} \left(e^{-N_{fi}} \frac{k}{H} \right) J_{1-\kappa_i/2} \left(e^{-N_{fi}} \frac{k}{H} \right) + J_{-1+\kappa_f/2} \left(e^{-N_{fi}} \frac{k}{H} \right) J_{-\kappa_i/2} \left(e^{-N_{fi}} \frac{k}{H} \right) \right), \end{aligned} \quad (3.20)$$

with

$$C = \frac{\pi}{2} e^{\frac{1}{2}N_{fi}(-2+\kappa_f-\kappa_i)} \frac{k}{H} \csc \left(\frac{\pi\kappa_f}{2} \right). \quad (3.21)$$

The matrix has the property $M(N_{fi}, \kappa_m, \kappa_f, k) \cdot M(N_{fi}, \kappa_i, \kappa_m, k) = M(N_{fi}, \kappa_i, \kappa_f, k)$, so that we can select the value $\kappa = 3$ as a reference point for all transitions between different values of κ .

One can also define a matrix corresponding to a “pulse” of height κ different from the value 3 corresponding to the scale-invariant case. The parameter η_{\parallel} is

$$\eta_{\parallel}(N) = \frac{3-\kappa}{2} (\Theta(N - N_1) - \Theta(N - N_2)) \quad (3.22)$$

and the corresponding matrix has the form

$$M_{\text{pulse}}(N_1, N_2, \kappa, k) = M(N_2, \kappa, 3, k) \cdot M(N_1, 3, \kappa, k). \quad (3.23)$$

A product of several M_{pulse} matrices can reproduce the final values of the coefficients (C_p, C_m) of the Bessel functions $J_{\pm 3/2}$ after the perturbations have evolved from an initial configuration corresponding to $(C_p, C_m) = (1, i)$ through a period of strong features. Clearly, it is possible to reconstruct any smooth function $\eta_{\parallel}(N)$ in terms of short intervals of N during which the function takes constant values. Multiplying the corresponding M_{pulse} matrices would provide a solution to the problem of the evolution of perturbations. The increase of the power spectrum relative to the scale invariant one is given by the final value of the coefficient $|C_m|^2$ after a mode of given k has evolved past the strong features in the background.

Simple analytic expressions can be obtained in the limits of large and small k , using the corresponding expansions of the Bessel functions. Keeping the leading contribution, one finds that the power spectrum is scale invariant at late times (or $N \rightarrow \infty$) for $k \rightarrow \infty$, but has a value multiplied

by the factor of eq. (3.17). The corrections subleading in H/k introduce oscillatory patterns in the spectrum [66].

Explicit expressions can be obtained for the case of a “pulse” of large positive amplitude (negative η_{\parallel}) and very short duration. For large positive values of κ and a short interval δN , we can approximate the Bessel function as

$$J_a(z) = \frac{1}{\Gamma(a+1)} \left(\frac{z}{2}\right)^a \left(1 - \frac{z^2}{4(1+a)} + \mathcal{O}(z^4)\right). \quad (3.24)$$

We find that

$$M_{\text{pulse}}^{(\text{sharp})}(N_1, k) = e^{N_1} \frac{H}{k} \begin{pmatrix} T_{11} & T_{12} \\ T_{21} & T_{22} \end{pmatrix} \left(1 + \mathcal{O}\left(\frac{1}{2\kappa} \left(e^{-N_1} \frac{k}{H}\right)^2\right)\right), \quad (3.25)$$

where

$$\begin{aligned} T_{11} &= \cos\left(e^{-N_1} \frac{k}{H}\right) \left(e^{-N_1} \frac{k}{H} \cos\left(e^{-N_1} \frac{k}{H}\right) - \sin\left(e^{-N_1} \frac{k}{H}\right)\right), \\ T_{12} &= \cos\left(e^{-N_1} \frac{k}{H}\right) \left(e^{-N_1} \frac{k}{H} \sin\left(e^{-N_1} \frac{k}{H}\right) + \cos\left(e^{-N_1} \frac{k}{H}\right)\right), \\ T_{21} &= \sin\left(e^{-N_1} \frac{k}{H}\right) \left(e^{-N_1} \frac{k}{H} \cos\left(e^{-N_1} \frac{k}{H}\right) - \sin\left(e^{-N_1} \frac{k}{H}\right)\right), \\ T_{22} &= \sin\left(e^{-N_1} \frac{k}{H}\right) \left(e^{-N_1} \frac{k}{H} \sin\left(e^{-N_1} \frac{k}{H}\right) + \cos\left(e^{-N_1} \frac{k}{H}\right)\right). \end{aligned} \quad (3.26)$$

For $k/H \lesssim e^{N_1} \sqrt{2\kappa}$ the presence of the “pulse” does not induce a suppression of the perturbation. The only effect is the introduction of oscillations in the spectrum. The spectrum is expected to have a deep minimum once per period, i.e. at intervals $\delta k/H = e^{N_1} \pi$. The suppression of the perturbation by $\exp(-\kappa \delta N)$ is expected to occur for $k/H \gtrsim e^{N_1} \sqrt{2\kappa}$.

After a step in the potential is crossed, the inflaton settles in a slow-roll regime on a flat part of the potential. During the approach to slow-roll, the evolution is dominated by the first two terms in the equation of motion of the background field: $\ddot{\phi} + 3H\dot{\phi} = 0$. This means that, during an interval $N_1 \leq N \leq N_2$, we have $\eta_{\parallel} \simeq 3$ and $\kappa = -3$. We can define the matrix

$$M_{\text{pulse}}^{(\text{negative})}(N_1, N_2, k) = M(N_2, -3, 3, k) \cdot M(N_1, 3, -3, k) \quad (3.27)$$

in order to account for the effect on the curvature perturbation, similarly to the treatment above. Then, the total effect on the coefficients of the Bessel functions, arising from crossing a step in the potential, is given by

$$\begin{pmatrix} C_{p_f} \\ C_{m_f} \end{pmatrix} = M_{\text{pulse}}^{(\text{negative})}(N_1, N_2, k) \cdot M_{\text{pulse}}^{(\text{sharp})}(N_1, k) \begin{pmatrix} 1 \\ i \end{pmatrix}. \quad (3.28)$$

The value of the spectrum relative to the scale-invariant case is determined by $|C_{m_f}|^2$. We can obtain an explicit expression for the enhancement of the spectrum by evaluating C_{m_f} through eq. (3.28), keeping the leading contribution for $M_{\text{pulse}}^{(\text{sharp})}(N_1, k)$. By defining $\tilde{k} = e^{-N_1} k/H$ and $\epsilon = \exp(-N_2 + N_1)$, we find

$$|C_{m_f}|^2 = \frac{1 + \tilde{k}^2}{4\epsilon^{12} \tilde{k}^{12}} \left(A_1 \sin(\tilde{k}) + A_2 \cos(\tilde{k}) + A_3 \sin(\tilde{k} - 2\epsilon\tilde{k}) + A_4 \cos(\tilde{k} - 2\epsilon\tilde{k})\right)^2, \quad (3.29)$$

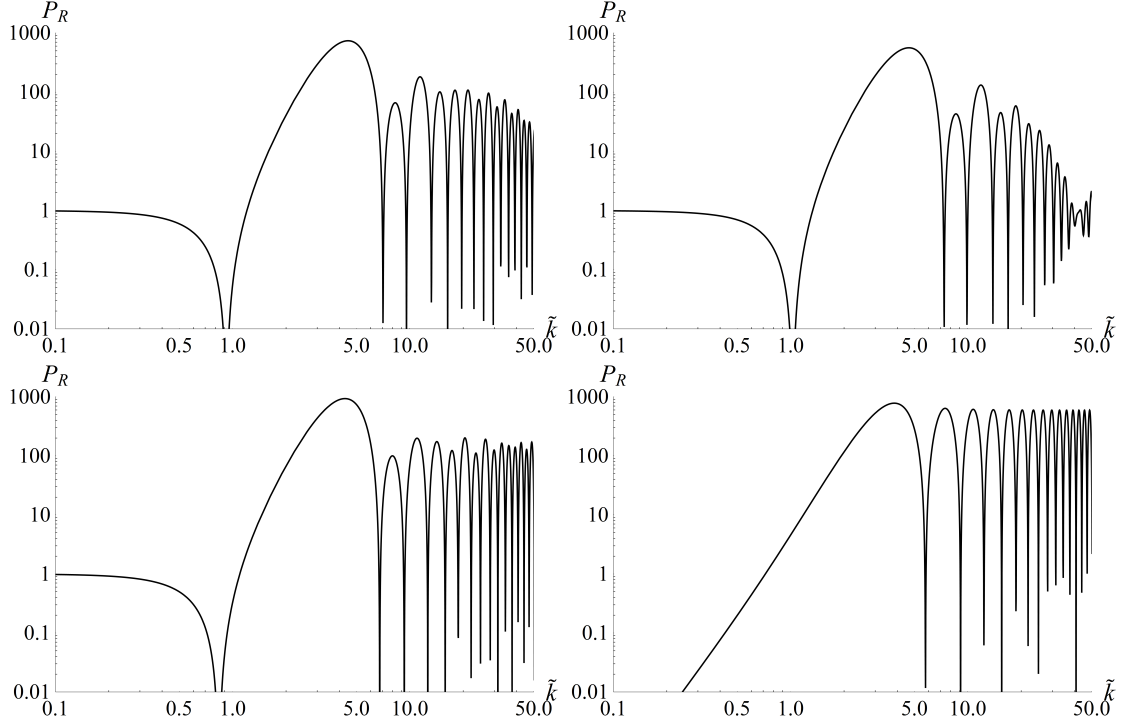


Figure 2. The power spectrum induced by a positive “pulse” of height κ between N_1 and N'_1 , followed by a negative “pulse” of height -3 between N'_1 and N_2 , as a function of $\tilde{k} = e^{-N_1} k/H$. Top row, left plot: $\kappa = 100$, $N_1 = 0$, $N'_1 = 0.05$, $N_2 = 0.858$. Top row, right plot: $\kappa = 50$, $N_1 = 0$, $N'_1 = 0.1$, $N_2 = 0.883$. Bottom row, left plot: The approximation of eq. (3.29) for $N_1 = 0$, $N_2 = 0.833$. Bottom row, right plot: The approximation of eq. (3.31) for $N_1 = 0$, $N_2 = 0.833$.

with

$$\begin{aligned}
A_1 &= 9\tilde{k} + 9\epsilon^2\tilde{k}^3 - 6\epsilon^3\tilde{k}^3 + 2\epsilon^3\tilde{k}^5 \\
A_2 &= 9 - 3\tilde{k}^2 + 9\epsilon^2\tilde{k}^2 - 3\epsilon^2\tilde{k}^4 + 6\epsilon^3\tilde{k}^4 \\
A_3 &= -9\tilde{k} + 18\epsilon\tilde{k} - 6\epsilon\tilde{k}^3 + 9\epsilon^2\tilde{k}^3 \\
A_4 &= -9 + 3\tilde{k}^2 - 18\epsilon\tilde{k}^2 + 9\epsilon^2\tilde{k}^2 - 3\epsilon^2\tilde{k}^4.
\end{aligned} \tag{3.30}$$

In order for a step to increase the spectrum by several orders of magnitude, one must have $N_2 - N_1 \gtrsim 1$. Modes with $e^{-N_1} k/H = \mathcal{O}(1)$ satisfy $e^{-N_2} k/H \ll 1$. In this momentum range we can expand eq. (3.29) in ϵ and keep the leading contribution

$$|C_{m_f}|^2 \simeq e^{6(N_2 - N_1)} \frac{4(1 + \tilde{k}^2)}{\tilde{k}^6} \left(3\tilde{k} \cos(\tilde{k}) + (-3 + \tilde{k}^2) \sin(\tilde{k}) \right)^2. \tag{3.31}$$

The enhancement is given by eq. (3.17), taking into account only the contribution from the negative “pulse” (positive η_{\parallel}). There is also oscillatory behaviour induced by sines and cosines of $\exp(-N_1)k/H$. The combined effect indicates that the power spectrum near its maximum is enhanced through the negative “pulse”, but also develops strong oscillations at intervals $\delta k/H = e^{N_1}\pi$. We emphasize that the expressions (3.29) and (3.31) are valid only near the maximum of the spectrum. They do not account for the expected drop of the spectrum for $e^{-N_1} k/H \gtrsim \sqrt{2\kappa}$, with κ the height of the positive sharp “pulse”.

In fig. 2 we test the accuracy of the various analytic results of this section in the case of square “pulses”, such as those depicted in fig. 1. The top row displays the spectra for two cases: a) a

positive “pulse” of height $\kappa = 100$ between $N_1 = 0$ and $N'_1 = 0.05$, followed by a negative “pulse” of height -3 between $N'_1 = 0.05$ and $N_2 = 0.858$, and b) a positive “pulse” of height $\kappa = 50$ between $N_1 = 0$ and $N'_1 = 0.1$, followed by a negative “pulse” of height -3 between $N'_1 = 0.1$ and $N_2 = 0.883$. These are simplified versions of the typical evolution of η_{\parallel} when the background inflaton crosses steps in the potential of variable steepness [65, 66]. The integrated area of the negative “pulse” is approximately the same in both cases, so that a comparable enhancement of the spectrum is expected. The spectra in the top row have been computed through the numerical solution of eq. (2.21), the system of eq. (3.13) and the expression of eq. (3.28). All these methods agree very well. The bottom row displays the approximation of eq. (3.29) (left plot) and the approximation of eq. (3.31) (right plot). Both these expressions assume $N'_1 \simeq N_1$, while they do not depend on the height κ of the positive “pulse”, as long as this is very large. We have used $N_1 = 0$, $N_2 = 0.833$. It is apparent that eq. (3.29) reproduces very well the form of the spectrum for $e^{-N_1} k/H \lesssim \sqrt{2\kappa}$. For larger values of k , the expected drop of the spectrum is not captured by this approximation. The deviation is clearer in the right plot, for which κ is smaller and the drop sets in earlier. On the other hand, eq. (3.31) is a cruder approximation. However, its simplicity makes it very useful for estimating the magnitude of the enhancement of the spectrum, as well as the fundamental frequency of oscillations.

3.3 Multiple features

In this subsection we examine the effect on the power spectrum of several “pulses” in the evolution of $\eta_{\parallel}(N)$. A similar effect has already been discussed in refs. [65, 66] through a numerical solution of eq. (2.21). We return to this issue here, making use of the approximation of eq. (3.19). A similar effect will be discussed in the following section, arising through η_{\perp} .

We specialize in the case of “pulses” generated through steps in the inflaton potential. The effect of one step is captured by the relation (3.28). In most cases one step is not sufficient to induce an enhancement of the spectrum by more than three or four orders of magnitude. It must be noted, however, that an enhancement by up to seven orders of magnitude is possible for an appropriately engineered potential and step profile [76]. The generalization to several steps is straightforward, through the inclusion of several M_{pulse} matrices, and can lead to further enhancement.

If fig. 3 we present spectra induced by one or more features in the evolution of η_{\parallel} , consisting of a positive “pulse” of height $\kappa = 50$ between $N_1 = 0$ and $N'_1 = 0.1$, followed by a negative “pulse” of height $\kappa = -3$ between $N'_1 = 0.1$ and $N_2 = 0.883$. We present four spectra, arising when one, two (top row), three or four (bottom row) such features occur, one immediately after the other. As has been discussed in refs. [65, 66], such features result from multiple steep steps in the inflaton potential. The spectra obtained for one feature are consistent with those derived through similar approaches [78, 79]. Moreover, it is apparent that multiple features act constructively, increasing the enhancement of the spectrum. A multitude of characteristic frequencies also appear through the dependence of the spectrum on combinations of the form $e^{-N_i} k/H$, with N_i corresponding to the time that a sharp transition occurs in the evolution of $\eta_{\parallel}(N)$.

It is important to note that the various sets of “pulses” should be placed close to each other for the enhancement of the power spectrum to be significant. Similarly, the corresponding steps in the inflaton potential must be close. If we increase the distance in efoldings between the sets of “pulses”, the additive effect is not as strong. Beyond a certain distance, each set acts independently on the spectrum, giving a moderate enhancement within a different k -range.

4 Turns in field space

In this section we turn to a different source of enhancement of the curvature spectrum, which is possible when the isocurvature perturbations become strongly excited during a finite period of

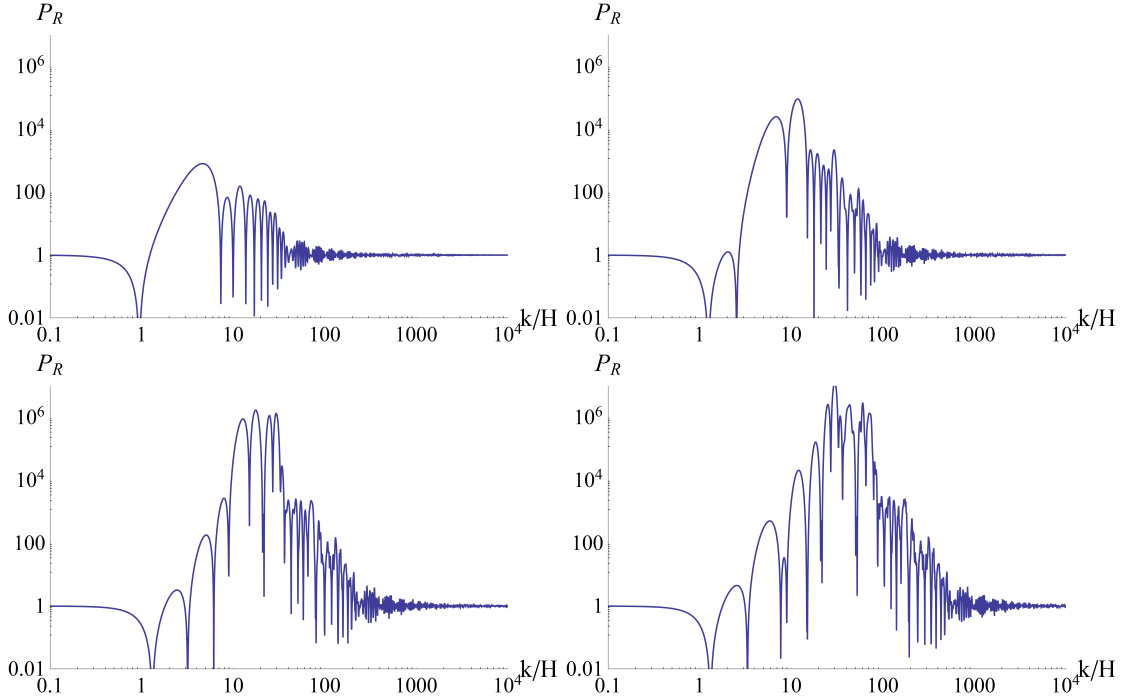


Figure 3. Power spectra induced by successive occurrences of a feature consisting of a positive “pulse” of height $\kappa = 50$ between $N_1 = 0$ and $N'_1 = 0.1$, followed by a negative “pulse” of height $\kappa = -3$ between $N'_1 = 0.1$ and $N_2 = 0.883$. Top row: one feature (left plot), two features (right plot). Bottom row: three features (left plot), four features (right plot).

efoldings and act as a source for the curvature perturbations. In the two-field case we discussed in section 2, this situation occurs when the parameter η_\perp satisfies $\eta_\perp^2 \gg M^2/H^2$, with M the typical mass of the mode perpendicular to the inflaton trajectory. The relevant equations are eqs. (2.22), (2.23). The evolution of the background can be rather complicated, depending on the characteristics of the two-field potential [40, 58]. We concentrate here on a simplified scenario, which preserves the relevant features without requiring a numerical calculation of the background evolution.

4.1 Maximal turn and multiple features

We consider models of a two-component field $\phi^a = (\chi, \psi)$ with a standard kinetic term, for which the curvature of the field manifold vanishes. We assume that the potential has an almost flat direction along a curve $\psi = f(\chi)$. A small constant slope along this direction results in a small value of the slow-roll parameter ϵ , which we assume to be constant. Along the perpendicular direction the potential has a large curvature, so that the flat direction forms a valley. We consider the simplest scenario, in which the fields evolve very close to the bottom of the valley, without perpendicular oscillations. We approximate the Hubble parameter as constant, with a value set by the average value of the potential along the flat direction. A particular realization of this setup, with $f(\chi) = a^2/\chi$, is given in ref. [40].

The unit vectors, tangential and normal to the valley at $\phi^a = (\chi, f(\chi))$, are

$$T^a = \frac{1}{\sqrt{1 + f'^2(\chi)}} (1, f'(\chi)) \quad (4.1)$$

$$N^a = \frac{1}{\sqrt{1 + f'^2(\chi)}} (f'(\chi), -1). \quad (4.2)$$

If we assume that the norm of $\dot{\phi}^a$ stays constant and equal to $\sqrt{2\epsilon}H$, we find that

$$\chi_{,N} = \pm \frac{\sqrt{2\epsilon}}{\sqrt{1+f'^2(\chi)}}. \quad (4.3)$$

We now have

$$T_{,N}^a = \frac{\partial T^a}{\partial \chi} \chi_{,N} = \frac{f''(\chi)}{(1+f'^2(\chi))^{3/2}} \chi_{,N} (-f'(\chi), 1) = -\frac{f''(\chi)}{1+f'^2(\chi)} \chi_{,N} N^a. \quad (4.4)$$

From eq. (2.15) we deduce that

$$\eta_{\perp} = \frac{f''(\chi)}{1+f'^2(\chi)} \chi_{,N} = \pm \sqrt{2\epsilon} \frac{f''(\chi)}{(1+f'^2(\chi))^{3/2}}. \quad (4.5)$$

It is apparent that η_{\perp} is nonzero only in regions in which $f''(\chi) \neq 0$, so that the valley of the potential is not linear.

We are interested in a scenario in which a linear part of the valley is succeeded by a sharp turn, leading to a second linear part. Without loss of generality we can assume that the turn is located near $\chi = \psi = 0$. The background evolution will be characterized by a short interval in which η_{\perp} will rise and fall sharply from zero. The angle of rotation in field space obeys $\theta_{,N} = \eta_{\perp}$, from which we obtain

$$\Delta\theta = \int_{N_i}^{N_f} \eta_{\perp}(\chi) dN = \int_{\chi_i}^{\chi_f} \frac{f''(\chi)}{1+f'^2(\chi)} d\chi = \arctan(f'(\chi)) \Big|_{\chi_i}^{\chi_f}. \quad (4.6)$$

The maximal angle can be obtained if $f'(\chi_i) \rightarrow -\infty$ before the turn and $f'(\chi_f) \rightarrow \infty$ after, so that $\Delta\theta = \pi$.

In the model of ref. [40], in which $f(\chi) = a^2/\chi$, one can have $f'(\chi_i) \rightarrow -\infty$ before the turn and $f'(\chi_f) \rightarrow 0$ after, so that $\Delta\theta = \pi/2$. The maximal value of η_{\perp} is obtained for $\chi = \psi = a$. It is $\eta_{\perp\text{max}} = \sqrt{\epsilon}/a$, and can be arbitrarily large for $a \rightarrow 0$. The duration of the turn is roughly $\Delta N \sim \Delta\theta/\eta_{\perp\text{max}} = \pi a/(2\sqrt{\epsilon})$ and can be very short for $a \rightarrow 0$.

As the value of the integral in eq. (4.6) is bounded by π , the effect of sharp turns on the amplification of the isocurvature and curvature perturbations is limited. However, multiple turns can also occur. The sign of the rotation angle is arbitrary, so a sequence of turns with alternating signs is possible. The enhancement of the curvature perturbation depends only on $|\eta_{\perp}|$, as can be easily seen through inspection of eqs. (2.22), (2.23). In fig. 4 we depict the typical evolution of η_{\perp} when the potential has several turns along its flat direction. We also present the approximation of the various features through ‘‘pulses’’, which we shall employ in the following. The integral over each feature must be smaller than π , so that the valley of the potential does not close on itself. This limits the possible enhancement arising from each turn. However, the combined effect of several turns can be substantial, as we show in this section.

4.2 The qualitative features of the evolution

As we discussed in section 2 the perturbations in the two-field system are governed by eqs. (2.22), (2.23). In order to simplify the picture, we assume that M is constant and $M/H \gtrsim 1$, so that the isocurvature modes get suppressed during the parts of the evolution in which η_{\perp} is small. However, when $\eta_{\perp} \gg M/H$ the evolution becomes non-trivial, as both the curvature and isocurvature modes get excited. The term $\sim \eta_{\perp}^2$ in the lhs of eq. (2.23) acts as a negative mass term, triggering the rapid growth of the field \mathcal{S}_k . As a result, the rhs of eq. (2.22) becomes a strong source term for the field \mathcal{R}_k . The resulting growth of \mathcal{R}_k generates a source term in the rhs of eq. (2.23) that moderates the maximal value of the field \mathcal{S}_k . The combined effect results in the enhancement of both modes. However, the late evolution of \mathcal{S}_k , when η_{\perp} becomes negligible, is dominated by its nonzero mass,

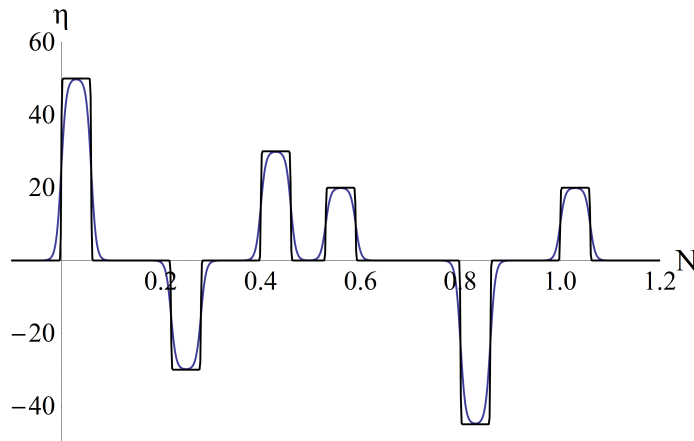


Figure 4. Typical evolution of the function $\eta_{\perp}(N)$ induced by turns in the inflaton potential. The approximation through “pulses” is also depicted.

so that this field eventually vanishes. The curvature mode \mathcal{R}_k freezes, similarly to the standard inflationary scenario, preserving its enhancement within a certain momentum range. Another characteristic consequence of the presence of strong features in the potential during inflation, is the appearance of distinctive oscillations in the curvature spectrum.

In order to obtain an analytic understanding of the evolution of the perturbations, we consider the “pulse” approximation of the previous section, in which η_{\perp} has the form

$$\eta_{\perp}(N) = \eta_{\perp 0} (\Theta(N - N_1) - \Theta(N - N_2)). \quad (4.7)$$

The parameter η_{\perp} takes a constant value for $N_1 < N < N_2$, and approaches zero very quickly outside this range. For $N < N_1$ and $N > N_2$ the two equations of motion decouple

$$\mathcal{R}_{k,NN} + 3\mathcal{R}_{k,N} + \frac{k^2}{H^2} e^{-2N} \mathcal{R}_k = 0 \quad (4.8)$$

$$\mathcal{S}_{k,NN} + 3\mathcal{S}_{k,N} + \frac{k^2}{H^2} e^{-2N} \mathcal{S}_k + \frac{M^2}{H^2} \mathcal{S}_k = 0, \quad (4.9)$$

resulting in simple solutions of the following form

$$\mathcal{R}_k(N) = e^{-3N/2} \left[C_p J_{\frac{3}{2}} \left(e^{-N} \frac{k}{H} \right) + C_m J_{-\frac{3}{2}} \left(e^{-N} \frac{k}{H} \right) \right] \quad (4.10)$$

$$\mathcal{S}_k(N) = e^{-3N/2} \left[D_p J_{\frac{1}{2}\sqrt{9-4M^2/H^2}} \left(e^{-N} \frac{k}{H} \right) + D_m J_{-\frac{1}{2}\sqrt{9-4M^2/H^2}} \left(e^{-N} \frac{k}{H} \right) \right]. \quad (4.11)$$

Initial conditions corresponding to the Bunch-Davies vacuum are obtained for $C_{p_i} = 1$, $C_{m_i} = i$. For the massive mode, the coefficients must be chosen more carefully, so that they reproduce the free-wave solution for $N \rightarrow -\infty$ when M becomes negligible. They read

$$D_{p_i} = -\sqrt{2}(1+i) \frac{e^{\frac{i\pi}{4}\sqrt{9-4M^2/H^2}}}{1 - e^{i\pi\sqrt{9-4M^2/H^2}}} e^{i\phi} \quad (4.12)$$

$$D_{m_i} = \sqrt{2}(1+i) \frac{e^{\frac{3i\pi}{4}\sqrt{9-4M^2/H^2}}}{1 - e^{i\pi\sqrt{9-4M^2/H^2}}} e^{i\phi}. \quad (4.13)$$

We have also included an arbitrary phase difference ϕ between the curvature and isocurvature modes at early times. This phase may affect the profile of the spectra by modifying the interference patterns

when the two modes interact. However, we have found that the quantitative conclusions about the spectrum enhancement and the characteristic oscillations it may display are largely unaffected. For this reason, we use $\phi = 0$ in our analysis.

The evolution in the interval $N_1 < N < N_2$ is complicated because of the coupling between the two modes. The main features are more clearly visible if we neglect the expansion of space, which is a good approximation for $\Delta N = N_2 - N_1 \lesssim 1$. The evolution equations now become

$$\mathcal{R}_{k,NN} + \frac{k^2}{H^2} \mathcal{R}_k + 2\eta_{\perp 0} \mathcal{S}_{k,N} = 0 \quad (4.14)$$

$$\mathcal{S}_{k,NN} + \left(\frac{k^2}{H^2} + \frac{M^2}{H^2} - \eta_{\perp 0}^2 \right) \mathcal{S}_k - 2\eta_{\perp 0} \mathcal{R}_{k,N} = 0. \quad (4.15)$$

Following refs. [33, 34], we look for solutions of the form

$$\mathcal{R}_k = A e^{\omega N}, \quad \mathcal{S}_k = B e^{\omega N}. \quad (4.16)$$

There are four independent solutions

$$\omega_i = \pm \frac{1}{\sqrt{2}} \sqrt{-\left(\frac{M^2}{H^2} + 3\eta_{\perp 0}^2 + 2\frac{k^2}{H^2}\right) \pm \sqrt{\left(\frac{M^2}{H^2} + 3\eta_{\perp 0}^2\right)^2 + 16\frac{k^2}{H^2}\eta_{\perp 0}^2}}, \quad (4.17)$$

with $i = 1, 2, 3, 4$ corresponding to the combinations of signs $++$, $-+$, $+-$, $--$, respectively. The corresponding values of B_i are

$$B_{1,2} = f_+ \omega_{1,2} A_{1,2} \quad (4.18)$$

$$B_{3,4} = f_- \omega_{3,4} A_{3,4}, \quad (4.19)$$

with

$$f_{\pm} = \frac{4\eta_{\perp 0}}{\frac{M^2}{H^2} - 5\eta_{\perp 0}^2 \pm \sqrt{\left(\frac{M^2}{H^2} + 3\eta_{\perp 0}^2\right)^2 + 16\frac{k^2}{H^2}\eta_{\perp 0}^2}}. \quad (4.20)$$

The solutions on either side of N_1 and N_2 can be matched, assuming the continuity of $\mathcal{R}_k(N)$, $\mathcal{S}_k(N)$ and $\mathcal{S}_{k,N}(N)$. The first derivative of $\mathcal{R}_k(N)$ must account for the δ -function arising from the derivative of $\eta_{\perp}(N)$ at these points. This leads to the conditions

$$\mathcal{R}_{k,N}(N_{1-}) = \mathcal{R}_{k,N}(N_{1+}) + 2\eta_{\perp 0} \mathcal{S}_k(N_1) \quad (4.21)$$

$$\mathcal{R}_{k,N}(N_{2-}) = \mathcal{R}_{k,N}(N_{2+}) - 2\eta_{\perp 0} \mathcal{S}_k(N_2). \quad (4.22)$$

For given initial conditions $C_{p_i}, C_{m_i}, D_{p_i}, D_{m_i}$ before the ‘‘pulse’’, one can calculate, through the use of these boundary conditions, the constants A_i within the ‘‘pulse’’, and eventually the final coefficients of the free solutions $C_{p_f}, C_{m_f}, D_{p_f}, D_{m_f}$ after the ‘‘pulse’’. In analogy to the previous section, one can thus determine the matrix M_{pulse} that links the solutions before and after the ‘‘pulse’’:

$$\begin{bmatrix} C_{p_f} \\ C_{m_f} \\ D_{p_f} \\ D_{m_f} \end{bmatrix} = M_{\text{pulse}}(N_1, N_2, k, M, \eta_{\perp}) \begin{bmatrix} C_{p_i} \\ C_{m_i} \\ D_{p_i} \\ D_{m_i} \end{bmatrix}. \quad (4.23)$$

This matrix facilitates calculations for more complex problems with multiple ‘‘pulses’’, occurring when the linear valley of the potential is interrupted by multiple, successive turns. Unfortunately, the expressions for the matrix elements are extensive and not very illuminating. For this reason we do not present them explicitly.

The influence of the “pulse” on the evolution of the perturbations can be inferred through inspection of eq. (4.17). Two of the solutions (ω_3 and ω_4) are purely imaginary, resulting in oscillatory behaviour. The other two (ω_1 and ω_2) have a more complicated dependence on the parameters of the problem. For $\frac{k}{H} \geq \sqrt{\eta_{\perp 0}^2 - \frac{M^2}{H^2}}$ they are imaginary as well, but for $\frac{k}{H} \leq \sqrt{\eta_{\perp 0}^2 - \frac{M^2}{H^2}}$ they become real, thus inducing exponential growth or suppression. In the limit $\Delta N \rightarrow 0$, $\eta_{\perp 0} \rightarrow \infty$, with the total area of the “pulse” (or total angle of the turn) $\Delta\theta = \eta_{\perp 0}\Delta N$ kept constant, we have

$$\omega_{1,2} = \pm \frac{k}{H\sqrt{3}} + \mathcal{O}(\Delta N). \quad (4.24)$$

We expect then that the spectrum will be enhanced by a factor

$$P_{\mathcal{R}} \sim \exp\left[\frac{2k}{H\sqrt{3}}\Delta N\right] = \exp\left[\frac{2\Delta\theta}{\sqrt{3}}\frac{k/H}{\eta_{\perp 0}}\right]. \quad (4.25)$$

The fact that the maximal turn $\Delta\theta$ cannot exceed π for canonical kinetic terms implies that the enhancement of the spectrum appears for scales k/H comparable to $\eta_{\perp 0}$. As the general solution is a superposition of all independent solutions (4.16), (4.17), the exponential growth is accompanied by oscillatory behaviour with a characteristic frequency set by $\eta_{\perp 0}$. For large k the spectrum returns to its scale-invariant form, as the effect of the “pulse” diminishes.

The constraint on $\Delta\theta$ implies that a single turn results only in limited growth of the spectrum [33]. However, multiple turns can have an additive, and often resonant, effect. In this respect it is important to point out another feature of the solutions. We are interested in the regime $\eta_{\perp 0} \gg M/H$, so that we can neglect the effect of the mass inside the “pulse”. For $k/H \ll \eta_{\perp 0}$, strong oscillations, with a frequency set by $\eta_{\perp 0}$, occur within the “pulse”. On the other hand, outside the “pulse” the characteristic frequency of oscillations, modulated by the expansion, is set by k or M . The continuity of $\mathcal{S}_k(N)$ and its derivative implies that the amplitude of oscillations increases significantly when the perturbation exits the “pulse”. The effect is visible if one matches at $N = 0$ the toy functions $f_i(N)$ and $f_f(N)$ given by

$$f_{i,f}(N) = A_{i,f}e^{-ik_{i,f}N} + B_{i,f}e^{ik_{i,f}N}. \quad (4.26)$$

This results in

$$\begin{aligned} A_f &= \frac{1}{2} \left(1 + \frac{k_i}{k_f}\right) A_i + \frac{1}{2} \left(1 - \frac{k_i}{k_f}\right) B_i \\ B_f &= \frac{1}{2} \left(1 - \frac{k_i}{k_f}\right) A_i + \frac{1}{2} \left(1 + \frac{k_i}{k_f}\right) B_i. \end{aligned} \quad (4.27)$$

For $k_i \ll k_f$, as when entering a “pulse”, the constants A_f , B_f are comparable to A_i , B_i , while for $k_i \gg k_f$, as when exiting a “pulse”, they are greatly enhanced. We shall see realizations of this effect in the two-field context through the numerical solution of eqs. (2.22), (2.23) in the following.

Before completing the subsection, we point out that the alternative formulation of the calculation of the spectrum that was introduced in section 3.1 for the single field case can be generalized for two fields. We present the relevant expressions in appendix B.

4.3 Numerical evaluation of the spectra

The precise form of the power spectrum in the two-field case is not captured easily through an analytic approach, especially when multiple features appear in the inflaton potential. For this reason, we resort to the numerical integration of eqs. (2.22), (2.23). In fig. 5 we present the evolution of the amplitude of perturbations $\mathcal{R}_k(N)$ and $\mathcal{S}_k(N)$ in two distinct cases. The perturbations are normalized so that the curvature spectrum is equal to 1 for $\eta_{\perp} = 0$.

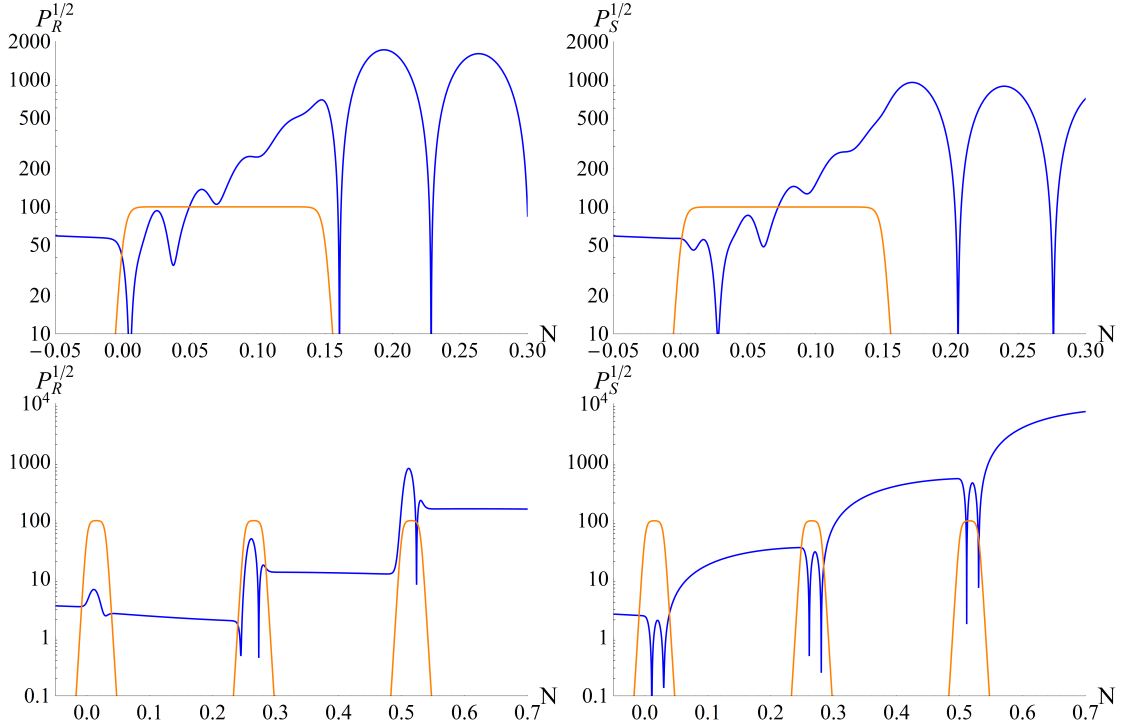


Figure 5. The evolution of the curvature mode (left plots) and isocurvature mode (right plots) for two types of time dependence for the parameter η_{\perp} : Top row: Thick “pulse”. Bottom row: A sequence of three narrow “pulses” of alternating sign. The function $|\eta_{\perp}(N)|$ is depicted. The mass of the isocurvature mode is $M/H = 5$. The momentum of both modes is $k/H \simeq 56$ in the top row and $k/H \simeq 3.2$ in the bottom row.

In the top row of fig. 5 we present $\mathcal{R}_k(N)$ (left plot) and $\mathcal{S}_k(N)$ (right plot) for a wide “pulse”, also depicted in the plots. This example does not represent a physical situation for vanishing curvature \mathbb{R} of the internal field manifold, because the total turn $\Delta\theta$ is approximately 15. It is presented in order to demonstrate the qualitative features discussed in the previous subsection, which become relevant for $\mathbb{R} \neq 0$. The mode momentum is $k/H \simeq 56$, of the same order as the height $\eta_{\perp 0} \simeq 100$ of the “pulse”. The mass of the isocurvature mode is $M/H \simeq 5$. One sees clearly the rapid growth of the perturbations inside the “pulse” and the appearance of oscillations with frequency set by $\eta_{\perp 0}$. After exiting the “pulse”, the perturbations oscillate with frequency set by k . For $N \rightarrow \infty$ (a region not depicted in the plots) the isocurvature mode asymptotically vanishes because of its nonzero mass. The curvature mode freezes when the horizon is crossed at a value larger than the one corresponding to the scale-invariant case ($\eta_{\perp} = 0$).

In the bottom row of fig. 5 we present the evolution in the case of multiple “pulses”. The width of each “pulse” is much smaller than in the previous example, so that each turn $-\Delta\theta$ — in field space is smaller than π . The turns have alternating signs and in the plot we depict $|\eta_{\perp}(N)|$. The mode momentum is $k/H \simeq 3.2$, much smaller than $\eta_{\perp 0}$. The mass of the isocurvature mode is again $M/H \simeq 5$. It is apparent that the growth of both modes within the “pulses” is not substantial, even though strong oscillations occur with frequency set by $\eta_{\perp 0}$. The distinctive feature is the strong increase of the amplitude of the isocurvature mode when the perturbation exits the “pulse”. This is expected, according to our discussion at the end of the previous subsection. The oscillation frequency for this mode outside the “pulses” is set by the mass and is rather low. The location of the “pulses” is such that a resonance effect occurs, with the amplitude of \mathcal{S}_k being amplified each time a “pulse” is traversed. This effect also triggers the growth of the curvature mode. The late

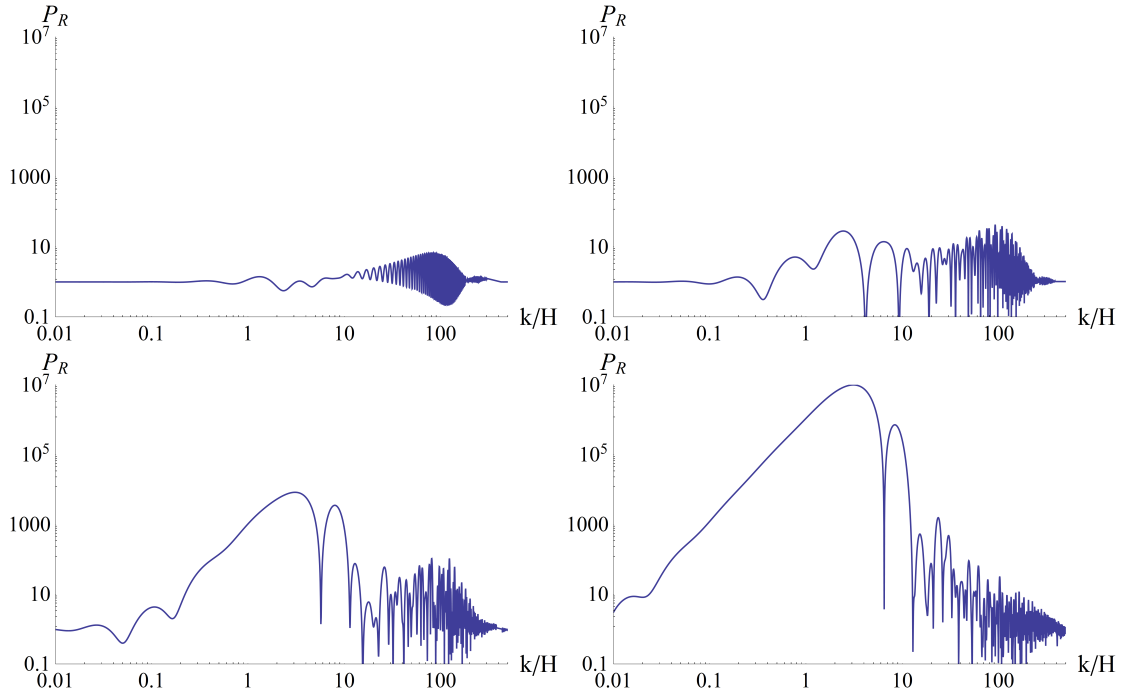


Figure 6. Curvature spectrum induced by a sequence of “pulses” of alternating signs in the function $\eta_{\perp}(N)$. Top row: one “pulse” (left), two “pulses” (right). Bottom row: three “pulses” (left), four “pulses” (right). We have kept the same scales for the axes in all plots for direct comparison.

time behaviour of both modes (not depicted in the plot) is similar to the previous case.

In fig. 6 we depict the form of the curvature spectrum induced by a function $\eta_{\perp}(N)$ displaying a sequence of “pulses” such as those in the bottom row of fig. 5. The “pulses” have alternating signs and are located at a distance of 0.25 efoldings from each other. Each “pulse” has a width of approximately 0.03 efoldings, a height $\eta_{\perp 0} \simeq 100$ and a total area smaller than π . We have used the same scales in all plots in order to be able to make direct visual comparisons. The top row includes the spectra generated by one (left plot) or two (right plot) “pulses”. The bottom row includes the spectra generated by three (left plot) or four (right plot) “pulses”. The spectra are normalized to the scale-invariant one. The location of the point $k/H = 1$ is arbitrary. It corresponds to the mode that crosses the horizon at the time at which we have set $N = 0$ for the number of efoldings, with N also taking negative values. In order to make contact with observations, the normalization of k must be set relative to the CMB scale.

In all plots we observe the enhancement of the spectrum in the region $k/H \sim \eta_{\perp 0}$. This enhancement increases with the number of “pulses”, but not to a significant degree. On the other hand, a strong enhancement appears for multiple “pulses” at low values of k/H , which increases dramatically with each addition of a “pulse”. This is the realization of the mechanism that we discussed above in relation to the bottom row of fig. 5. The resonance effect appears for $1/k$ comparable to the distance between the “pulses”. For our plot we kept this distance fixed. However, similar patterns in the spectrum are obtained for variable locations of the “pulses”, as long as their separations are comparable. The exact height of each “pulse” may also vary. It must be noted that the effect is strongly amplified by very sharp “pulses”. We have chosen profiles that match the form of $\eta_{\perp}(N)$ expected by models such as the one we discussed in subsection 4.1.

5 GWs and the PBH counterpart

Primordial inhomogeneities imprinted on the CMB are limited to scales of order larger than a Mpc. Large enhancements of the power spectrum of perturbations on small scales, such as those produced through the mechanisms discussed in this paper, are not directly visible on the CMB sky due to photon diffusion damping. A new method to probe small-scale perturbations is the search for a stochastic GW background, see ref. [80] for a recent review. The LIGO-Virgo-KAGRA collaboration has already given us some first constraints [19].

The stochastic GWs are sourced by the primordial density perturbations. Part of the energy stored in the perturbations is released via gravitational radiation at the moment of horizon reentry. These are second-order tensor modes generated by first-order scalar modes [67–70]. The power spectrum of the secondary, or induced, GWs is expressed in a compact form as a double integral involving the power spectrum of the curvature perturbations:

$$\overline{\mathcal{P}_h(\tau, k)} = \int_0^\infty dt \int_{-1}^1 ds \mathcal{T}(s, t, \tau, k) \mathcal{P}_{\mathcal{R}}\left(\frac{t+s+1}{2}k\right) \mathcal{P}_{\mathcal{R}}\left(\frac{t-s+1}{2}k\right). \quad (5.1)$$

The overline denotes the oscillation average and $\mathcal{T}(s, t, \tau, k)$ is a kernel function. In this section we are describing the evolution in terms of the conformal time τ . The variables t and s are defined as $t = u + v - 1$, $s = u - v$, where $v = q/k$, $u = |\mathbf{k} - \mathbf{q}|/k$. Further details can be found in ref. [81]. Under radiation domination, most of the growth of the induced-GW amplitude occurs rapidly, during a period $\tau_c \sim O(10) k_{\text{peak}}^{-1}$, with k_{peak} the location of the peak of $\mathcal{P}_{\mathcal{R}}$. After this time the GWs propagate freely. They have a fractional spectral energy density given by the GW energy density ρ_{GW} relative to the critical or total energy density ρ_{tot} per logarithmic wavenumber interval

$$\Omega_{\text{GW}}(\tau, k) = \frac{1}{\rho_{\text{tot}}(\tau)} \frac{d\rho_{\text{GW}}(\tau, k)}{d \ln k} = \frac{1}{24} \left(\frac{k}{a(\tau)H(\tau)} \right)^2 \overline{\mathcal{P}_h(\tau, k)}. \quad (5.2)$$

At the present time τ_0 , the dimensionless spectral density of GWs is

$$\Omega_{\text{GW}}(\tau_0, f)h^2 = 0.39 \times \left(\frac{g_*}{106.75} \right)^{-1/3} \Omega_{\text{rad},0}h^2 \times \Omega_{\text{GW}}(\tau_c, f), \quad (5.3)$$

where $\Omega_{\text{rad},0}h^2 = 4.2 \times 10^{-5}$, τ_0 the age of the universe today, and τ_c the time at which most of the GW production takes place. The total energy density parameter is obtained by integrating the GW energy density spectrum over the entire frequency interval.

As a rule of thumb, for a scalar spectrum described by a log-normal type distribution $\mathcal{P}_{\mathcal{R}}(k) = \mathcal{P}_{\mathcal{R}}(k_{\text{peak}})e^{-(z/\sigma)^2}$, with amplitude $\mathcal{P}_{\mathcal{R}}(k_{\text{peak}})$ at a narrow peak, $z \equiv \ln(k/k_{\text{peak}})$ and σ the width of the distribution, the GW spectral energy density today features a peak with amplitude $\Omega_{\text{GW}}(\tau_0, f_{\text{peak}})h^2 \sim 10^{-5}\sigma^2\mathcal{P}_{\mathcal{R}}^2(k_{\text{peak}})$ [82, 83]. A curvature power spectrum with peak amplitude $\mathcal{P}_{\mathcal{R}} \sim 10^{-2}$ induces a GW peak with $\Omega_{\text{GW}}(\tau_0, f_{\text{peak}}) \sim 10^{-9}\sigma^2$, while $\mathcal{P}_{\mathcal{R}} \sim 10^{-4}$ induces a GW peak with $\Omega_{\text{GW}}(\tau_0, f_{\text{peak}}) \sim 10^{-13}\sigma^2$. Both values are in the range of sensitivity of designed GW detectors [84], such as LISA [13, 14] and DECIGO [15]. The width σ of the $\mathcal{P}_{\mathcal{R}}(k)$ peak is characteristic of each model and shapes the $\Omega_{\text{GW}}(\tau_0, f)$ spectrum.

The enhancement of the curvature power spectrum due to several “pulses” in the evolution of η_{\parallel} generates a GW spectrum with a characteristic peak structure, discussed in ref. [66]. The main peak of the curvature spectrum is found to be narrow, $\sigma < 1$, and induces a GW spectrum with a major peak after a flat plateau. Additional oscillatory patterns are superimposed on this main peak, reflecting the strong oscillations in the curvature spectrum depicted in fig. 3. A similar general peak structure is found for a “pulse” in the evolution of η_{\perp} , see Fig. 7. However, in this case the subleading oscillatory patterns are located after the main peak, which remains fairly smooth.

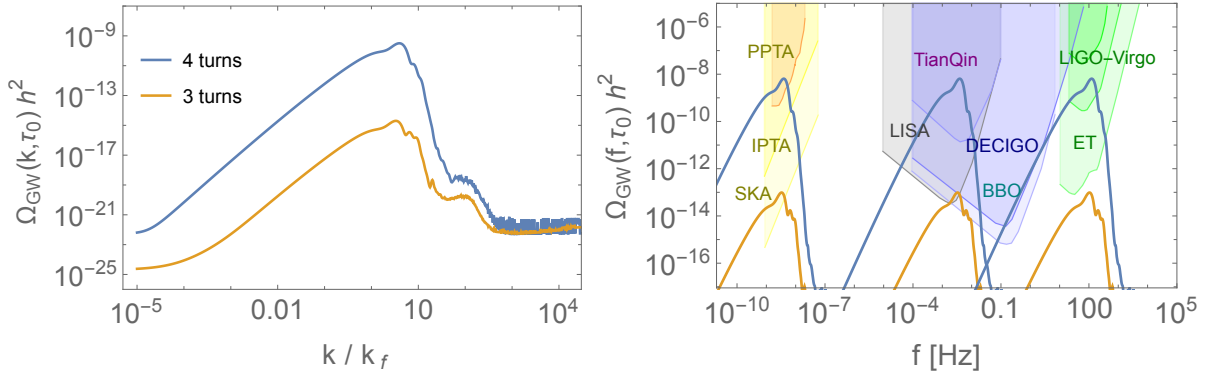


Figure 7. *Left plot:* The GW spectral density produced by inflationary trajectories with 3 and 4 successive turns occurring at the wavenumber k_f . The scale k_f is the scale that crosses the horizon at the time when the first feature occurs. In the right plot, we select three different values for this scale. *Right plot:* The GW spectra placed at three benchmark frequencies that lie within the range of sensitivity of current and near future GW experiments.

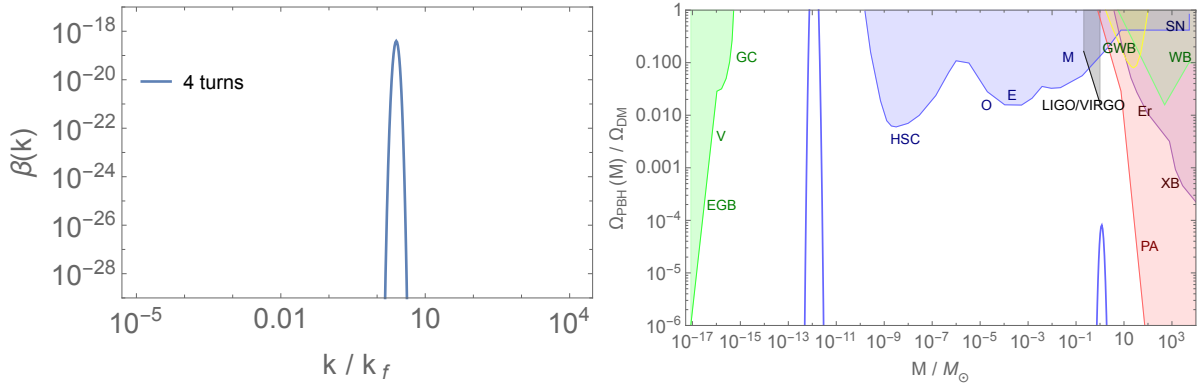


Figure 8. *Left plot:* The β mass fraction produced by an inflationary trajectory with four successive turns occurring at the wavenumber k_f . *Right plot:* The corresponding fractional PBH abundance against the observational constraints [71], with masses placed at benchmark scales that can be probed by current and near future GW experiments. These are the same scales used for the right plot of fig. 7. The right curve corresponds to the left spectrum in fig. 7, the left curve to the middle spectrum, while the right spectrum in fig. 7 corresponds to very small black holes that have evaporated by today.

This is a consequence of the smooth form of the main peak of the curvature spectrum depicted in fig. 6.

In order to make contact with physical scales we must eliminate the ambiguity in the definition of N . For this we can use the scale k_f that crosses the horizon at the time N_f when the first feature occurs. In the approximation of constant H that we are using, we have $k_f = e^{N_f} H$. This allows us to eliminate H in favour of k_f , and express every other scale as $k/k_f = e^{\delta N}$, with $\delta N = N - N_f$. In the previous sections we were setting $N_f = 0$, unless stated otherwise. Notice that varying N_f is equivalent to varying k_f and allows us to place the peak of the spectrum at a desired value. As a result, the GW spectrum can be shifted along the frequency axis, in order to check its detectability depending on the time of occurrence of the feature that causes the enhancement, as is done in the right plot of fig. 7.

The amplification of the spectrum with respect to the CMB scale depends on the number of

turns, their size and sharpness. We considered turns smaller than π and “pulses” of amplitude $|\eta_{\perp}| \lesssim 100$. Different configurations can produce an enhancement of the curvature spectrum $\mathcal{P}_{\mathcal{R}}$ of similar size. For example, a configuration of four turns of angular size $\lesssim \pi$ described by four pulses of size $|\eta_{\perp}| \sim 100$ that last $\Delta N \sim 0.1$ can enhance the power spectrum by a factor of 10^7 . A similar enhancement is produced by a configuration of eight turns of size $\lesssim \pi/2$ described by eight pulses of size $|\eta_{\perp}| \sim 10$. Although each configuration produces a different spectral shape, the relative differences are not that evident. The curvature spectrum generally exhibits a major narrow peak, as can be seen in fig. 6, which creates a characteristic GW spectral peak, common for different configurations. The differences appear at $k > k_{\text{peak}}$ and correspond to complicated oscillatory patterns. These are reflected in the GW spectra of fig. 7 in frequency regions of lower amplitude.

Primordial curvature perturbations with large amplitudes at certain scales induce, apart from tensor modes, a gravitational collapse of sufficiently dense regions that enter the Hubble horizon. The mass fraction of PBHs at the formation time, $\beta(M)$, has an acute sensitivity to the amplitude of the power spectrum $\mathcal{P}_{\mathcal{R}}$. For the spherically symmetric gravitational collapse of a fluid with pressure, this sensitivity is exponential, $\beta \propto \sqrt{\mathcal{P}_{\mathcal{R}}} e^{-\delta_c^2/\mathcal{P}_{\mathcal{R}}}$, where δ_c is the density threshold for PBH formation. A sizable PBH abundance is obtained for $\mathcal{P}_{\mathcal{R}} \sim 10^{-2}$. The parameter β can increase if the background pressure is decreased, as for example during the QCD phase transition [85, 86]. A further decrease of the pressure to vanishing values can affect the PBH formation rate significantly [87, 88] and induce GW signals with different spectral density [89, 90].

In our set-up, large amplitudes of $\mathcal{P}_{\mathcal{R}}$ can be produced if several strong features, turns or steps, occur during the inflationary trajectory. These features can give an observable result in the GW channel for three or more successive turns. In Fig. 7 we plot the spectral density of the induced GWs for curvature power spectra that have the form depicted in Fig. 6. In figure 8 we plot the corresponding PBH abundance for a threshold value $\delta_c = 0.41$, together with the PBH experimental upper bounds [71]. For four turns the PBHs produced can constitute a significant fraction of the dark matter in the universe. We recall that during radiation domination the PBH mass spectrum is related to the $\mathcal{P}_{\mathcal{R}}$ peak position k_{peak} as $M_{\text{PBH}} \propto k_{\text{peak}}^{-2}$, and the PBHs have abundance $\Omega_{\text{PBH}} \propto \beta M_{\text{PBH}}^{-1/2}$, see Ref. [91] for details. PBHs in the mass range $M \sim 10^{-12} M_{\odot}$ can constitute the entire dark matter in the universe, while the associated GWs will be probed by LISA [12] and other future space GW antennas. PBHs with mass $M_{\text{PBH}} \gtrsim M_{\odot}$ can form binaries and are directly detectable by LIGO-Virgo-KAGRA experiments, while the associated induced GWs can be probed by PTA experiments [8–11]. The LIGO-Virgo-KAGRA collaboration already constrains the stochastic GW background [19] in the frequency band $\mathcal{O}(1 - 10^2)$ Hz, even though PBHs associated with these frequencies are too light to survive in the late universe.

6 Summary and conclusions

In this paper we extended our previous work [65, 66] on the enhancement of the curvature spectrum during inflation to the two-field case. The main emphasis of our analysis was on the resonant effect that may occur when there are several instances with strong deviations from approximate scale invariance during the inflationary evolution. We did not study a particular model, but looked instead for generic properties of the equations of motion for the perturbations which would lead to their enhancement. We identified the slow-roll parameter η as the quantity that can trigger the rapid growth of perturbations. In the two-field case that we analysed in this work, this parameter can be projected onto the directions parallel and perpendicular to the trajectory of the background fields. The corresponding two components, η_{\parallel} and η_{\perp} , remain small during most of the evolution, apart from short intervals during which they can take large, positive or negative, values.

The typical underlying reason for the appearance of strong features in the evolution of η_{\parallel} is the presence of points in the inflaton potential that cannot support slow-roll, such as sharp steps or inflection points. We focused mostly on the behaviour induced by sharp steps, even though our formalism can be applied to inflection points as well. The acceleration of the background inflaton when a step in the potential is crossed makes η_{\parallel} attain very negative values initially, followed by positive values when the inflaton settles in a slow-roll regime on a plateau following the step. The first part of the evolution is very short for sharp steps, while the second lasts longer with $\eta_{\parallel} \simeq 3$. During this second part, η_{\parallel} acts as negative friction, leading to the rapid growth of the curvature perturbation.

On the other hand, η_{\perp} grows large during sharp turns in field space. The typical situation involves an inflaton potential that contains an almost flat valley, with straight parts interrupted by sharp turns. The evolution along the valley satisfies the slow-roll conditions, apart from the short intervals during which the fields go through the turns and η_{\perp} takes large values, positive or negative, depending on the direction of the turn. The effect of η_{\perp} is sign-independent and twofold: a) it triggers the strong growth of the perturbation perpendicular to the trajectory (the isocurvature mode), and b) couples the isocurvature mode to the curvature mode along the trajectory, thus inducing its growth as well.

The focal point of our analysis was the additive effect of several features leading to the resonant growth of the curvature spectrum. Typical spectra arising when the enhancement comes through η_{\parallel} are presented in fig. 3. Three or four strong features are sufficient to produce an enhancement by six or seven orders of magnitude. A clear characteristic of the spectrum is the presence of strong oscillations, even around the peak, which reflect the characteristic times at which the features in the evolution of η_{\parallel} appear. When the enhancement comes through η_{\perp} , the resulting spectra have the typical form presented in fig. 6. Again, three or four features in the evolution of η_{\perp} are sufficient in order to induce an enhancement of the power spectrum by six or seven orders of magnitude. However, the spectrum now displays a smooth main peak, followed by a region of strong oscillatory behaviour. This form is a result of the mechanism that leads to the growth of the isocurvature perturbations, discussed in subsections 4.2 and 4.3 and depicted in fig. 5. It must be pointed out that the constructive interference of several features is affected by their separation, as discussed in subsection 4.3. The resonance effect appears for $1/k$ comparable to the distance between the “pulses”.

Apart from inducing the CMB anisotropies, inflation is a causal mechanism that can seed PBH formation and GW production in the early universe. Given the fact that we are largely ignorant of the form of the primordial curvature power spectrum at small scales, it is legitimate to consider every possibility about its amplitude. Non-minimal scenarios, such as those with turns, generate non-flat shapes with prominent peaks. These can lead to PBH and GW production, as we discussed in section 5. In order that a detectable GW background is produced, e.g. within the sensitivity range of LISA, three or more successive turns have to occur, while a significant PBH abundance requires at least four sharp turns. The scenario with several steps in the potential also leads to similar conclusions, as has been discussed in detail in refs. [65, 66]. A comparison of the corresponding GW spectra demonstrates that they both display a prominent maximum that may be localized within the range of sensitivity of designed GW detectors [84], such as LISA [13, 14] and DECIGO [15]. The difference between GW spectra produced through the presence of several features in η_{\parallel} and those produced through similar features in η_{\perp} lies in the secondary maxima that are present around the main peak in the first case, while they are absent in the second case. Their identification depends crucially on the data resolution of the various experiments. However, in principle they provide a means for probing the mechanism that generates the enhancement of the spectrum.

A big part of our study focused on the attempt to understand the evolution of the perturbations

and the resulting spectra through analytic means. This is a very difficult task, especially in the presence of several features in the background evolution, because of the complexity of the problem as it is reflected in the form of the evolution equations. We employed two different approaches:

- In the first approach we reformulated the problem using Green’s functions, deriving integral equations such as eq. (3.6) for the case of a non-trivial η_{\parallel} and eqs. (B.4), (B.5) for η_{\perp} . These can be used as a starting point for successive approximations, such as eqs. (3.8) and (3.15), (3.16), depicted and discussed in fig. 9. Expressions, such as eq. (3.8) provide intuition on the various frequencies of the oscillations that appear in the power spectrum, while eqs. (3.15), (3.16) give estimates of the amplitude of the spectrum far beyond linear perturbation theory. Exploiting this approach even further, we reformulated the evolution equations as a system of differential equations for the coefficients of an expansion of the general solution in terms of Bessel functions: eq. (3.10) in the η_{\parallel} case and eqs. (B.6), (B.7) in the η_{\perp} case. This formulation permits the analysis of non-minimal initial conditions in a straightforward manner and can reduce computational time.
- In the second approach, we approximated the features in the evolution of η as square “pulses” and used appropriate matching conditions at the beginning and end of each “pulse” in order to obtain a complete solution. For the case of a non-trivial η_{\parallel} , this approach resulted in the approximate expressions derived in subsection 3.2 and depicted in fig. 2. For the case of η_{\perp} we used the approximations suggested in refs. [33, 34] in order to understand the growth of the isocurvature perturbations within a single “pulse” and compare it with the situation for a sequence of “pulses”.

The broader picture that emerges from our analysis is that the observable consequences of inflation can be much more complex than what is suggested by the standard analysis that assumes small deviations from scale invariance for the whole range of scales of the primordial spectrum. The possibility that multiple features may be present in the background evolution points to a paradigm with richer physical behaviour, which is also more natural in the multi-field case. It is exciting that the critical examination of such speculations is within the reach of experiment.

Acknowledgments

The work of I. Dalianis, G. Kodaxis, and N. Tetradis was supported by the Hellenic Foundation for Research and Innovation (H.F.R.I.) under the “First Call for H.F.R.I. Research Projects to support Faculty members and Researchers and the procurement of high-cost research equipment grant” (Project Number: 824).

A Accuracy of the analytical estimates

In this appendix we provide an assessment of the accuracy of the approximate expressions (3.8) and (3.16). For the matrix $C(N)$, defined in eq. (3.16), we obtain

$$C_{11}(\infty) = 2 \int_{-\infty}^{\infty} \eta_{\parallel}(n) \sin\left(e^{-n} \frac{k}{H}\right) \left[e^n \frac{H}{k} \cos\left(e^{-n} \frac{k}{H}\right) + \sin\left(e^{-n} \frac{k}{H}\right) \right] dn \quad (\text{A.1})$$

$$C_{12}(\infty) = -2 \int_{-\infty}^{\infty} \eta_{\parallel}(n) \cos\left(e^{-n} \frac{k}{H}\right) \left[e^n \frac{H}{k} \cos\left(e^{-n} \frac{k}{H}\right) + \sin\left(e^{-n} \frac{k}{H}\right) \right] dn \quad (\text{A.2})$$

$$C_{21}(\infty) = 2 \int_{-\infty}^{\infty} \eta_{\parallel}(n) \sin\left(e^{-n} \frac{k}{H}\right) \left[e^n \frac{H}{k} \sin\left(e^{-n} \frac{k}{H}\right) - \cos\left(e^{-n} \frac{k}{H}\right) \right] dn \quad (\text{A.3})$$

$$C_{22}(\infty) = -2 \int_{-\infty}^{\infty} \eta_{\parallel}(n) \cos\left(e^{-n} \frac{k}{H}\right) \left[e^n \frac{H}{k} \sin\left(e^{-n} \frac{k}{H}\right) - \cos\left(e^{-n} \frac{k}{H}\right) \right] dn, \quad (\text{A.4})$$

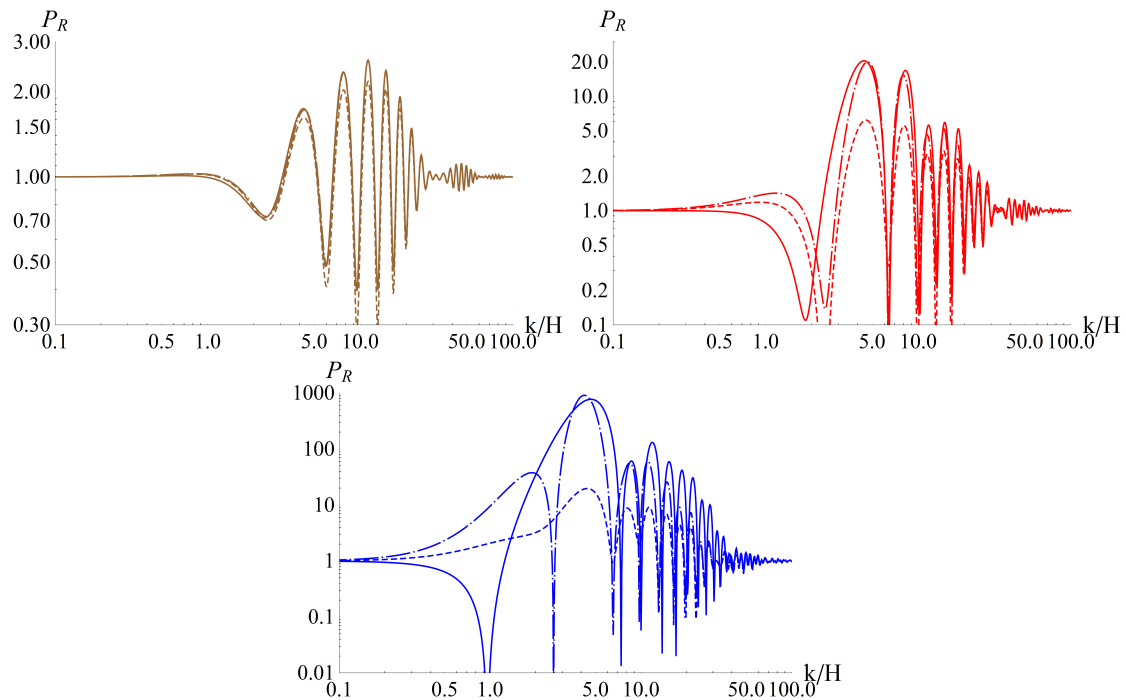


Figure 9. Power spectra for the three different smooth curves of fig. 1. The solid curves correspond to the exact numerical solution of eq. (2.21) or the system (3.13). The short-dashed curves correspond to the approximation of eq. (3.8), and the long-dashed curves to the approximation of eq. (3.16). Notice the large difference in the vertical scales of the three plots.

where we have used appropriate partial integrations. The first two terms in a Taylor expansion of the exponential give an estimate for $E(\infty)$ that reproduces the approximate result of eq. (3.8). Additional terms account for higher-order corrections. These improve the convergence for slowly varying functions $\eta_{||}(N)$. However, for functions $\eta_{||}(N)$ that induce an enhancement of the spectrum by several orders of magnitude, the quantitative accuracy of this approach is limited.

In order to check the validity of the approximate expressions (3.8) and (3.16), we consider a sequence of typical patterns of the function $\eta_{||}(N)$, similar to those induced by step steps in the inflaton potential [65, 66]. The form of $\eta_{||}(N)$ is depicted in fig. 1 and discussed in the main text.

In fig. 9 we depict the power spectra for the three different smooth curves of fig. 1. The solid curves correspond to the exact numerical solution of eq. (2.21) or the system (3.13). The short-dashed curves correspond to the approximation of eq. (3.8), and the long-dashed curves to the approximation of eq. (3.16). We are interested only in relatively strong deviations from scale invariance, and not in the absolute normalization of the spectrum. For this reason we have assumed that the spectrum is scale invariant at early and late times and normalized with respect to its value in these regions. It is apparent from fig. 9 that both approximations give a very accurate description of the spectrum when its value is of order 1. When the spectrum is significantly enhanced both approximations lose accuracy. However, eq. (3.16) gives a reasonable approximation to the maximal value of the spectrum and its characteristic frequencies, even for an enhancement by three orders of magnitude.

B An alternative formulation in the two-field case

The differential equations (2.22), (2.23) can be turned into integral equations through the use of the appropriate Green's functions. For the curvature mode, the Green's function is given by eq. (3.3). For the massive isocurvature mode, the generalization is straightforward and the retarded Green's function $\bar{G}_k(n, N)$ for $n < N$ is

$$\bar{G}_{k<}(N, n) = e^{-3N/2} \left(P(n) J_{\frac{1}{2}\sqrt{9-4M^2/H^2}} \left(e^{-N} \frac{k}{H} \right) + Q(n) J_{-\frac{1}{2}\sqrt{9-4M^2/H^2}} \left(e^{-N} \frac{k}{H} \right) \right), \quad (\text{B.1})$$

with

$$P(n) = -\frac{\pi}{2} e^{3n/2} \csc \left(\frac{\pi}{2} \sqrt{9-4M^2/H^2} \right) J_{-\frac{1}{2}\sqrt{9-4M^2/H^2}} \left(e^{-N} \frac{k}{H} \right) \quad (\text{B.2})$$

$$Q(n) = \frac{\pi}{2} e^{3n/2} \csc \left(\frac{\pi}{2} \sqrt{9-4M^2/H^2} \right) J_{\frac{1}{2}\sqrt{9-4M^2/H^2}} \left(e^{-N} \frac{k}{H} \right). \quad (\text{B.3})$$

Hence, the general solution can be expressed as:

$$\mathcal{R}_k(N) = \bar{\mathcal{R}}_k(N) - 2 \int_{-\infty}^N G_{k<}(N, n) \left(\frac{\partial}{\partial n} (\eta_{\perp}(n) \mathcal{S}_k(n)) + 3\eta_{\perp}(n) \mathcal{S}_k(n) \right) dn \quad (\text{B.4})$$

$$\mathcal{S}_k(N) = \bar{\mathcal{S}}_k(N) + \int_{-\infty}^N \bar{G}_{k<}(N, n) (\eta_{\perp}^2(n) \mathcal{S}_k(n) + 2\eta_{\perp}(n) \mathcal{R}_{k,n}(n)), \quad (\text{B.5})$$

where $\bar{\mathcal{S}}_k(N)$, $\bar{\mathcal{R}}_k(N)$ are the homogeneous solutions.

The form of the above equations suggests the ansatz

$$\mathcal{R}_k(N) = e^{-3N/2} \left(D(N) J_{3/2} \left(e^{-N} \frac{k}{H} \right) + E(N) J_{-3/2} \left(e^{-N} \frac{k}{H} \right) \right) \quad (\text{B.6})$$

$$\mathcal{S}_k(N) = e^{-3N/2} \left(K(N) J_{\frac{1}{2}\sqrt{9-4M^2/H^2}} \left(e^{-N} \frac{k}{H} \right) + L(N) J_{-\frac{1}{2}\sqrt{9-4M^2/H^2}} \left(e^{-N} \frac{k}{H} \right) \right) \quad (\text{B.7})$$

By substituting in the derivative of eqs. (B.4), (B.5), and matching the coefficients of the Bessel functions, we obtain a system of four first-order differential equations:

$$\frac{\partial}{\partial N} \begin{bmatrix} D(N) \\ E(N) \\ K(N) \\ L(N) \end{bmatrix} = F(N) \begin{bmatrix} D(N) \\ E(N) \\ K(N) \\ L(N) \end{bmatrix} \quad (\text{B.8})$$

where $F(N)$ is a 4×4 matrix with nonzero elements $F_{ij}(N)$ given by

$$\begin{aligned}
F_{11}(N) &= F_{12}(N) = F_{21}(N) = F_{22}(N) = 0 \\
F_{13}(N) &= 2e^{-3N/2}\eta_{\perp}(N)(A'(N) - 3A(N))J_{\frac{1}{2}\sqrt{9-4M^2/H^2}}\left(e^{-N}\frac{k}{H}\right) \\
F_{14}(N) &= 2e^{-3N/2}\eta_{\perp}(N)(A'(N) - 3A(N))J_{-\frac{1}{2}\sqrt{9-4M^2/H^2}}\left(e^{-N}\frac{k}{H}\right) \\
F_{23}(N) &= 2e^{-3N/2}\eta_{\perp}(N)(B'(N) - 3B(N))J_{\frac{1}{2}\sqrt{9-4M^2/H^2}}\left(e^{-N}\frac{k}{H}\right) \\
F_{24}(N) &= 2e^{-3N/2}\eta_{\perp}(N)(B'(N) - 3B(N))J_{-\frac{1}{2}\sqrt{9-4M^2/H^2}}\left(e^{-N}\frac{k}{H}\right) \\
F_{31}(N) &= -2e^{-3N/2}\frac{d}{dN}(\eta_{\perp}(N)P(N))J_{\frac{3}{2}}\left(e^{-N}\frac{k}{H}\right) \\
F_{32}(N) &= -2e^{-3N/2}\frac{d}{dN}(\eta_{\perp}(N)P(N))J_{-\frac{3}{2}}\left(e^{-N}\frac{k}{H}\right) \\
F_{33}(N) &= e^{-3N/2}\eta_{\perp}^2(N)P(N)J_{\frac{1}{2}\sqrt{9-4M^2/H^2}}\left(e^{-N}\frac{k}{H}\right) \\
F_{34}(N) &= e^{-3N/2}\eta_{\perp}^2(N)P(N)J_{-\frac{1}{2}\sqrt{9-4M^2/H^2}}\left(e^{-N}\frac{k}{H}\right) \\
F_{41}(N) &= -2e^{-3N/2}\frac{d}{dN}(\eta_{\perp}(N)Q(N))J_{\frac{3}{2}}\left(e^{-N}\frac{k}{H}\right) \\
F_{42}(N) &= -2e^{-3N/2}\frac{d}{dN}(\eta_{\perp}(N)Q(N))J_{-\frac{3}{2}}\left(e^{-N}\frac{k}{H}\right) \\
F_{43}(N) &= e^{-3N/2}\eta_{\perp}^2(N)Q(N)J_{\frac{1}{2}\sqrt{9-4M^2/H^2}}\left(e^{-N}\frac{k}{H}\right) \\
F_{44}(N) &= e^{-3N/2}\eta_{\perp}^2(N)Q(N)J_{-\frac{1}{2}\sqrt{9-4M^2/H^2}}\left(e^{-N}\frac{k}{H}\right). \tag{B.9}
\end{aligned}$$

This system of equations must be solved with initial conditions at $N \rightarrow -\infty$. For the Bunch-Davies vacuum $(D, E) = (1, i)$, while (K, L) are given by eqs. (4.12), (4.13).

References

- [1] V. F. Mukhanov and G. V. Chibisov, ‘‘Quantum Fluctuations and a Nonsingular Universe,’’ *JETP Lett.* **33** (1981), 532-535;
- [2] S. W. Hawking, ‘‘The Development of Irregularities in a Single Bubble Inflationary Universe,’’ *Phys. Lett. B* **115** (1982), 295;
- [3] A. A. Starobinsky, ‘‘Dynamics of Phase Transition in the New Inflationary Universe Scenario and Generation of Perturbations,’’ *Phys. Lett. B* **117** (1982), 175-178;
- [4] A. H. Guth and S. Y. Pi, ‘‘Fluctuations in the New Inflationary Universe,’’ *Phys. Rev. Lett.* **49** (1982), 1110-1113
- [5] Y. Akrami *et al.* [Planck], ‘‘Planck 2018 results. X. Constraints on inflation,’’ *Astron. Astrophys.* **641** (2020), A10 [arXiv:1807.06211 [astro-ph.CO]].
- [6] <https://www.skatelescope.org>
- [7] <http://ipta4gw.org>
- [8] G. Hobbs, A. Archibald, Z. Arzoumanian, D. Backer, M. Bailes, N. D. R. Bhat, M. Burgay, S. Burke-Spolaor, D. Champion and I. Cognard, *et al.* ‘‘The international pulsar timing array

- project: using pulsars as a gravitational wave detector,” *Class. Quant. Grav.* **27** (2010), 084013 [arXiv:0911.5206 [astro-ph.SR]].
- [9] G. Janssen, G. Hobbs, M. McLaughlin, C. Bassa, A. T. Deller, M. Kramer, K. Lee, C. Mingarelli, P. Rosado and S. Sanidas, *et al.* “Gravitational wave astronomy with the SKA,” *PoS AASKA14* (2015), 037 [arXiv:1501.00127 [astro-ph.IM]].
- [10] L. Lentati, S. R. Taylor, C. M. F. Mingarelli, A. Sesana, S. A. Sanidas, A. Vecchio, R. N. Caballero, K. J. Lee, R. van Haasteren and S. Babak, *et al.* “European Pulsar Timing Array Limits On An Isotropic Stochastic Gravitational-Wave Background,” *Mon. Not. Roy. Astron. Soc.* **453** (2015) no.3, 2576-2598 [arXiv:1504.03692 [astro-ph.CO]].
- [11] Z. Arzoumanian *et al.* [NANOGrav], “The NANOGrav 12.5 yr Data Set: Search for an Isotropic Stochastic Gravitational-wave Background,” *Astrophys. J. Lett.* **905** (2020) no.2, L34 [arXiv:2009.04496 [astro-ph.HE]].
- [12] <https://www.elisascience.org>.
- [13] P. Amaro-Seoane *et al.* [LISA], “Laser Interferometer Space Antenna,” [arXiv:1702.00786 [astro-ph.IM]].
- [14] E. Barausse, E. Berti, T. Hertog, S. A. Hughes, P. Jetzer, P. Pani, T. P. Sotiriou, N. Tamanini, H. Witek and K. Yagi, *et al.* “Prospects for Fundamental Physics with LISA,” *Gen. Rel. Grav.* **52** (2020) no.8, 81 [arXiv:2001.09793 [gr-qc]].
- [15] S. Kawamura, M. Ando, N. Seto, S. Sato, M. Musha, I. Kawano, J. Yokoyama, T. Tanaka, K. Ioka and T. Akutsu, *et al.* “Current status of space gravitational wave antenna DECIGO and B-DECIGO,” *PTEP* **2021** (2021) no.5, 05A105 [arXiv:2006.13545 [gr-qc]].
- [16] W. H. Ruan, Z. K. Guo, R. G. Cai and Y. Z. Zhang, “Taiji program: Gravitational-wave sources,” *Int. J. Mod. Phys. A* **35** (2020) no.17, 2050075 [arXiv:1807.09495 [gr-qc]].
- [17] J. Luo *et al.* [TianQin], “TianQin: a space-borne gravitational wave detector,” *Class. Quant. Grav.* **33** (2016) no.3, 035010 [arXiv:1512.02076 [astro-ph.IM]].
- [18] L. Badurina, E. Bentine, D. Blas, K. Bongs, D. Bortoletto, T. Bowcock, K. Bridges, W. Bowden, O. Buchmueller and C. Burrage, *et al.* “AION: An Atom Interferometer Observatory and Network,” *JCAP* **05** (2020), 011 [arXiv:1911.11755 [astro-ph.CO]].
- [19] R. Abbott *et al.* [KAGRA, Virgo and LIGO Scientific], “Upper limits on the isotropic gravitational-wave background from Advanced LIGO and Advanced Virgo’s third observing run,” *Phys. Rev. D* **104** (2021) no.2, 022004 [arXiv:2101.12130 [gr-qc]].
- [20] M. Maggiore, C. Van Den Broeck, N. Bartolo, E. Belgacem, D. Bertacca, M. A. Bizouard, M. Branchesi, S. Clesse, S. Foffa and J. García-Bellido, *et al.* “Science Case for the Einstein Telescope,” *JCAP* **03** (2020), 050 [arXiv:1912.02622 [astro-ph.CO]].
- [21] A. A. Starobinsky and J. Yokoyama, “Density fluctuations in Brans-Dicke inflation,” [arXiv:gr-qc/9502002 [gr-qc]].
- [22] M. Sasaki and E. D. Stewart, “A General analytic formula for the spectral index of the density perturbations produced during inflation,” *Prog. Theor. Phys.* **95** (1996), 71-78 [arXiv:astro-ph/9507001 [astro-ph]].
- [23] J. Garcia-Bellido and D. Wands, “Metric perturbations in two field inflation,” *Phys. Rev. D* **53** (1996), 5437-5445 [arXiv:astro-ph/9511029 [astro-ph]].
- [24] A. D. Linde and V. F. Mukhanov, “Nongaussian isocurvature perturbations from inflation,” *Phys. Rev. D* **56** (1997), R535-R539 [arXiv:astro-ph/9610219 [astro-ph]].
- [25] D. Langlois, “Correlated adiabatic and isocurvature perturbations from double inflation,” *Phys. Rev. D* **59** (1999), 123512 [arXiv:astro-ph/9906080 [astro-ph]].

- [26] C. Gordon, D. Wands, B. A. Bassett and R. Maartens, “Adiabatic and entropy perturbations from inflation,” *Phys. Rev. D* **63** (2000), 023506 [arXiv:astro-ph/0009131 [astro-ph]].
- [27] S. Tsujikawa and H. Yajima, “New constraints on multifield inflation with nonminimal coupling,” *Phys. Rev. D* **62** (2000), 123512 [arXiv:hep-ph/0007351 [hep-ph]].
- [28] A. D. Linde, “Generation of Isothermal Density Perturbations in the Inflationary Universe,” *Phys. Lett. B* **158** (1985), 375-380
- [29] L. A. Kofman, “What Initial Perturbations May Be Generated in Inflationary Cosmological Models,” *Phys. Lett. B* **173** (1986), 400-404
- [30] D. Polarski and A. A. Starobinsky, “Isocurvature perturbations in multiple inflationary models,” *Phys. Rev. D* **50** (1994), 6123-6129 [arXiv:astro-ph/9404061 [astro-ph]].
- [31] V. F. Mukhanov and P. J. Steinhardt, “Density perturbations in multifield inflationary models,” *Phys. Lett. B* **422** (1998), 52-60 [arXiv:astro-ph/9710038 [astro-ph]].
- [32] S. Pi, Y. I. Zhang, Q. G. Huang and M. Sasaki, “Scalaron from R^2 -gravity as a heavy field,” *JCAP* **05** (2018), 042 [arXiv:1712.09896 [astro-ph.CO]].
- [33] G. A. Palma, S. Sypsas and C. Zenteno, “Seeding primordial black holes in multifield inflation,” *Phys. Rev. Lett.* **125** (2020) no.12, 121301 [arXiv:2004.06106 [astro-ph.CO]].
- [34] J. Fumagalli, S. Renaux-Petel and L. T. Witkowski, “Oscillations in the stochastic gravitational wave background from sharp features and particle production during inflation,” *JCAP* **08** (2021), 030 [arXiv:2012.02761 [astro-ph.CO]].
- [35] M. Braglia, X. Chen and D. K. Hazra, “Probing Primordial Features with the Stochastic Gravitational Wave Background,” *JCAP* **03** (2021), 005 [arXiv:2012.05821 [astro-ph.CO]].
- [36] A. Achúcarro, J. O. Gong, S. Hardeman, G. A. Palma and S. P. Patil, “Features of heavy physics in the CMB power spectrum,” *JCAP* **01** (2011), 030 [arXiv:1010.3693 [hep-ph]].
- [37] A. Achúcarro, J. O. Gong, S. Hardeman, G. A. Palma and S. P. Patil, “Mass hierarchies and non-decoupling in multi-scalar field dynamics,” *Phys. Rev. D* **84** (2011), 043502 [arXiv:1005.3848 [hep-th]].
- [38] X. Chen, “Primordial Features as Evidence for Inflation,” *JCAP* **01** (2012), 038 [arXiv:1104.1323 [hep-th]].
- [39] G. Shiu and J. Xu, “Effective Field Theory and Decoupling in Multi-field Inflation: An Illustrative Case Study,” *Phys. Rev. D* **84** (2011), 103509 [arXiv:1108.0981 [hep-th]].
- [40] S. Cespedes, V. Atal and G. A. Palma, “On the importance of heavy fields during inflation,” *JCAP* **05** (2012), 008 [arXiv:1201.4848 [hep-th]].
- [41] A. Avgoustidis, S. Cremonini, A. C. Davis, R. H. Ribeiro, K. Turzynski and S. Watson, “Decoupling Survives Inflation: A Critical Look at Effective Field Theory Violations During Inflation,” *JCAP* **06** (2012), 025 [arXiv:1203.0016 [hep-th]].
- [42] X. Gao, D. Langlois and S. Mizuno, “Influence of heavy modes on perturbations in multiple field inflation,” *JCAP* **10** (2012), 040 [arXiv:1205.5275 [hep-th]].
- [43] A. Achúcarro, J. O. Gong, G. A. Palma and S. P. Patil, “Correlating features in the primordial spectra,” *Phys. Rev. D* **87** (2013) no.12, 121301 [arXiv:1211.5619 [astro-ph.CO]].
- [44] M. Konieczka, R. H. Ribeiro and K. Turzynski, “The effects of a fast-turning trajectory in multiple-field inflation,” *JCAP* **07** (2014), 030 [arXiv:1401.6163 [astro-ph.CO]].
- [45] A. R. Brown, “Hyperbolic Inflation,” *Phys. Rev. Lett.* **121** (2018) no.25, 251601 [arXiv:1705.03023 [hep-th]].
- [46] A. Achúcarro, E. J. Copeland, O. Iarygina, G. A. Palma, D. G. Wang and Y. Welling, “Shift-symmetric orbital inflation: Single field or multifield?,” *Phys. Rev. D* **102** (2020) no.2, 021302

- [arXiv:1901.03657 [astro-ph.CO]].
- [47] J. Fumagalli, S. Garcia-Saenz, L. Pinol, S. Renaux-Petel and J. Ronayne, “Hyper-Non-Gaussianities in Inflation with Strongly Nongeodesic Motion,” *Phys. Rev. Lett.* **123** (2019) no.20, 201302 [arXiv:1902.03221 [hep-th]].
- [48] T. Bjorkmo, “Rapid-Turn Inflationary Attractors,” *Phys. Rev. Lett.* **122** (2019) no.25, 251301 [arXiv:1902.10529 [hep-th]].
- [49] P. Christodoulidis, D. Roest and E. I. Sfakianakis, “Scaling attractors in multi-field inflation,” *JCAP* **12** (2019), 059 [arXiv:1903.06116 [hep-th]].
- [50] M. Braglia, D. K. Hazra, F. Finelli, G. F. Smoot, L. Sriramkumar and A. A. Starobinsky, “Generating PBHs and small-scale GWs in two-field models of inflation,” *JCAP* **08** (2020), 001 [arXiv:2005.02895 [astro-ph.CO]].
- [51] Y. Aldabergenov, A. Addazi and S. V. Ketov, “Primordial black holes from modified supergravity,” *Eur. Phys. J. C* **80** (2020) no.10, 917 [arXiv:2006.16641 [hep-th]].
- [52] J. Fumagalli, S. Renaux-Petel, J. W. Ronayne and L. T. Witkowski, “Turning in the landscape: a new mechanism for generating Primordial Black Holes,” [arXiv:2004.08369 [hep-th]].
- [53] L. Iacconi, H. Assadullahi, M. Fasiello and D. Wands, “Revisiting small-scale fluctuations in α -attractor models of inflation,” [arXiv:2112.05092 [astro-ph.CO]].
- [54] A. J. Tolley and M. Wyman, “The Gelaton Scenario: Equilateral non-Gaussianity from multi-field dynamics,” *Phys. Rev. D* **81** (2010), 043502 [arXiv:0910.1853 [hep-th]].
- [55] S. Cremonini, Z. Lalak and K. Turzynski, “Strongly Coupled Perturbations in Two-Field Inflationary Models,” *JCAP* **03** (2011), 016 [arXiv:1010.3021 [hep-th]].
- [56] A. Achucarro, J. O. Gong, S. Hardeman, G. A. Palma and S. P. Patil, “Effective theories of single field inflation when heavy fields matter,” *JHEP* **05** (2012), 066 [arXiv:1201.6342 [hep-th]].
- [57] S. Pi and M. Sasaki, “Curvature Perturbation Spectrum in Two-field Inflation with a Turning Trajectory,” *JCAP* **10** (2012), 051 [arXiv:1205.0161 [hep-th]].
- [58] A. Achucarro, V. Atal, S. Cespedes, J. O. Gong, G. A. Palma and S. P. Patil, “Heavy fields, reduced speeds of sound and decoupling during inflation,” *Phys. Rev. D* **86** (2012), 121301 [arXiv:1205.0710 [hep-th]].
- [59] J. Fumagalli, G. A. Palma, S. Renaux-Petel, S. Sypsas, L. T. Witkowski and C. Zenteno, “Primordial gravitational waves from excited states,” [arXiv:2111.14664 [astro-ph.CO]].
- [60] X. Chen, “Primordial Non-Gaussianities from Inflation Models,” *Adv. Astron.* **2010** (2010), 638979 [arXiv:1002.1416 [astro-ph.CO]].
- [61] J. Chluba, J. Hamann and S. P. Patil, “Features and New Physical Scales in Primordial Observables: Theory and Observation,” *Int. J. Mod. Phys. D* **24** (2015) no.10, 1530023 [arXiv:1505.01834 [astro-ph.CO]].
- [62] A. Slosar, K. N. Abazajian, M. Abidi, P. Adshead, Z. Ahmed, D. Alonso, M. A. Amin, B. Ansarnejad, R. Armstrong and C. Baccigalupi, *et al.* “Scratches from the Past: Inflationary Archaeology through Features in the Power Spectrum of Primordial Fluctuations,” *Bull. Am. Astron. Soc.* **51** (2019) no.3, 98 [arXiv:1903.09883 [astro-ph.CO]].
- [63] G. D’Amico and N. Kaloper, “Rollercoaster cosmology,” *JCAP* **08** (2021), 058 [arXiv:2011.09489 [hep-th]].
- [64] V. C. Spanos and I. D. Stamou, “Gravitational waves and primordial black holes from supersymmetric hybrid inflation,” *Phys. Rev. D* **104** (2021) no.12, 123537 [arXiv:2108.05671 [astro-ph.CO]].
- [65] K. Kefala, G. P. Kodaxis, I. D. Stamou and N. Tetradis, “Features of the inflaton potential and the

- power spectrum of cosmological perturbations,” *Phys. Rev. D* **104** (2021) no.2, 023506 [arXiv:2010.12483 [astro-ph.CO]].
- [66] I. Dalianis, G. P. Kodaxis, I. D. Stamou, N. Tetradis and A. Tsigkas-Kouvelis, “Spectrum oscillations from features in the potential of single-field inflation,” *Phys. Rev. D* **104** (2021) no.10, 103510 [arXiv:2106.02467 [astro-ph.CO]].
- [67] S. Mollerach, D. Harari and S. Matarrese, “CMB polarization from secondary vector and tensor modes,” *Phys. Rev. D* **69** (2004), 063002 [arXiv:astro-ph/0310711 [astro-ph]].
- [68] K. N. Ananda, C. Clarkson and D. Wands, “The Cosmological gravitational wave background from primordial density perturbations,” *Phys. Rev. D* **75** (2007), 123518 [arXiv:gr-qc/0612013 [gr-qc]].
- [69] D. Baumann, P. J. Steinhardt, K. Takahashi and K. Ichiki, “Gravitational Wave Spectrum Induced by Primordial Scalar Perturbations,” *Phys. Rev. D* **76** (2007), 084019 [arXiv:hep-th/0703290 [hep-th]].
- [70] R. Saito and J. Yokoyama, “Gravitational wave background as a probe of the primordial black hole abundance,” *Phys. Rev. Lett.* **102** (2009), 161101 [erratum: *Phys. Rev. Lett.* **107** (2011), 069901] [arXiv:0812.4339 [astro-ph]].
- [71] B. Carr, K. Kohri, Y. Sendouda and J. Yokoyama, “Constraints on primordial black holes,” *Rept. Prog. Phys.* **84** (2021) no.11, 116902 [arXiv:2002.12778 [astro-ph.CO]].
- [72] J. Garcia-Bellido and E. Ruiz Morales, “Primordial black holes from single field models of inflation,” *Phys. Dark Univ.* **18** (2017), 47-54 [arXiv:1702.03901 [astro-ph.CO]].
- [73] C. Germani and T. Prokopec, “On primordial black holes from an inflection point,” *Phys. Dark Univ.* **18** (2017), 6-10 [arXiv:1706.04226 [astro-ph.CO]].
- [74] H. Motohashi and W. Hu, “Primordial Black Holes and Slow-Roll Violation,” *Phys. Rev. D* **96** (2017) no.6, 063503 [arXiv:1706.06784 [astro-ph.CO]].
- [75] I. Dalianis, A. Kehagias and G. Tringas, “Primordial black holes from α -attractors,” *JCAP* **01** (2019), 037 [arXiv:1805.09483 [astro-ph.CO]].
- [76] K. Inomata, E. McDonough and W. Hu, “Amplification of Primordial Perturbations from the Rise or Fall of the Inflaton,” [arXiv:2110.14641 [astro-ph.CO]].
- [77] G. Ballesteros, J. Beltran Jimenez and M. Pieroni, “Black hole formation from a general quadratic action for inflationary primordial fluctuations,” *JCAP* **06** (2019), 016 [arXiv:1811.03065 [astro-ph.CO]].
- [78] O. Özsoy and G. Tasinato, “On the slope of the curvature power spectrum in non-attractor inflation,” *JCAP* **04** (2020), 048 [arXiv:1912.01061 [astro-ph.CO]].
- [79] G. Tasinato, “An analytic approach to non-slow-roll inflation,” *Phys. Rev. D* **103** (2021) no.2, 023535 [arXiv:2012.02518 [hep-th]].
- [80] G. Domènech, “Scalar Induced Gravitational Waves Review,” *Universe* **7** (2021) no.11, 398 [arXiv:2109.01398 [gr-qc]].
- [81] K. Kohri and T. Terada, “Semianalytic calculation of gravitational wave spectrum nonlinearly induced from primordial curvature perturbations,” *Phys. Rev. D* **97** (2018) no.12, 123532 [arXiv:1804.08577 [gr-qc]].
- [82] I. Dalianis and K. Kritos, “Exploring the Spectral Shape of Gravitational Waves Induced by Primordial Scalar Perturbations and Connection with the Primordial Black Hole Scenarios,” *Phys. Rev. D* **103** (2021) no.2, 023505 [arXiv:2007.07915 [astro-ph.CO]].
- [83] S. Pi and M. Sasaki, “Gravitational Waves Induced by Scalar Perturbations with a Lognormal Peak,” *JCAP* **09** (2020), 037 [arXiv:2005.12306 [gr-qc]].
- [84] E. Thrane and J. D. Romano, “Sensitivity curves for searches for gravitational-wave backgrounds,”

- Phys. Rev. D **88** (2013) no.12, 124032 [arXiv:1310.5300 [astro-ph.IM]].
- [85] K. Jedamzik, “Primordial black hole formation during the QCD epoch,” Phys. Rev. D **55** (1997), 5871-5875 [arXiv:astro-ph/9605152 [astro-ph]].
- [86] C. T. Byrnes, M. Hindmarsh, S. Young and M. R. S. Hawkins, “Primordial black holes with an accurate QCD equation of state,” JCAP **08** (2018), 041 [arXiv:1801.06138 [astro-ph.CO]].
- [87] T. Harada, C. M. Yoo and K. Kohri, “Threshold of primordial black hole formation,” Phys. Rev. D **88** (2013) no.8, 084051 [erratum: Phys. Rev. D **89** (2014) no.2, 029903] [arXiv:1309.4201 [astro-ph.CO]].
- [88] T. Harada, C. M. Yoo, K. Kohri, K. i. Nakao and S. Jhingan, “Primordial black hole formation in the matter-dominated phase of the Universe,” Astrophys. J. **833** (2016) no.1, 61 [arXiv:1609.01588 [astro-ph.CO]].
- [89] K. Jedamzik, M. Lemoine and J. Martin, “Generation of gravitational waves during early structure formation between cosmic inflation and reheating,” JCAP **04** (2010), 021 [arXiv:1002.3278 [astro-ph.CO]].
- [90] I. Dalianis and C. Kouvaris, “Gravitational waves from density perturbations in an early matter domination era,” JCAP **07** (2021), 046 [arXiv:2012.09255 [astro-ph.CO]].
- [91] M. Sasaki, T. Suyama, T. Tanaka and S. Yokoyama, “Primordial black holes—perspectives in gravitational wave astronomy,” Class. Quant. Grav. **35** (2018) no.6, 063001 [arXiv:1801.05235 [astro-ph.CO]].